

1 **Developing a tile drainage module for Cold Regions**
2 **Hydrological Model: Lessons from a farm in Southern**
3 **Ontario, Canada**

4

5 Mazda Kompanizare^{*&#}, Diogo Costa⁺, Merrin L. Macrae[&], John W. Pomeroy^{*}, Richard M. Petrone[&]

6 ^{*}Centre for Hydrology, University of Saskatchewan, Canmore and Saskatoon, Canada

7 ⁺University of Évora, Mediterranean Institute for Agriculture, Environment and Development, Portugal

8 [&]University of Waterloo, Waterloo, Canada

9 [#]Corresponding author: kompanizare.mazda@usask.ca

10

11 **Abstract**

12 Systematic tile drainage is used extensively in agricultural lands to remove excess water and
13 improve crop growth; however, tiles can also transfer nutrients from farmlands to downstream
14 surface water bodies, leading to water quality problems. Thus, there is a need to simulate the
15 hydrological behaviour of tile drains to understand the impacts of climate or land management
16 change on agricultural runoff. The Cold Regions Hydrological Model (CRHM) is a physically
17 based, modular modeling system developed for cold regions. Here, a tile drainage module is
18 developed for CRHM. A multi-variable, multi-criteria model performance evaluation strategy
19 was deployed to examine the ability of the module to capture tile discharge under both winter
20 and summer conditions (NSE>0.29, RSR<0.84 and PBias <20 for tile flow and water table
21 simulations). Initial model simulations run at a 15-min interval did not satisfactorily represent

22 tile discharge; however, model simulations improved when the time step was refined to hourly
23 but also with the explicit representation of capillary rise for moisture interactions between the
24 rooting zone and groundwater, demonstrating the significance of capillary rise in the hydrology
25 of tile drains in loam soils. Novel aspects of this module include the shorter time step relative to
26 some existing models, which may enable future water quality modules to be added, and the use
27 of field capacity and its corresponding pressure head to provide estimates of drainable water and
28 the thickness of the capillary fringe, rather using than detailed soil retention curves that may not
29 always be available. An additional novel aspect of our results is the demonstration that flows in
30 some tile drain systems can be better represented and simulated when related to shallow
31 groundwater dynamics.

32

33 Keywords: tile drainage, cold regions, hydrological model, capillary fringe, drainable water,
34 water level fluctuations

35

36

37 **1. Introduction**

38

39 Harmful algal blooms and eutrophication in large freshwater lakes surrounded by agricultural
40 lands are major environmental challenges in Canada and globally. The transport of nutrients,
41 particularly phosphorus, in runoff from agricultural fields into rivers, ponds and eventually lakes
42 is an important contributor to the increased frequency of algal blooms being experienced in
43 North America and elsewhere (Sharpley et al., 1995; Correll, 1998; Filippelli, 2002; Ruttenberg,
44 2005; Schindler, 2006; Quinton et al., 2010; Costa et al., 2022). Nutrient transport from

45 agricultural fields can occur via both surface runoff and tile drainage (Radcliffe et al., 2015), and
46 recent increases in the frequency and magnitude of algal blooms in Lake Erie in North America
47 have been attributed to tile drainage (King et al., 2015; Jarvie et al., 2017). Tile drain systems
48 reduce the retention time of soil water, lessening waterlogging in fields and improving both crop
49 growth and field trafficability for farmers (Cordeiro and Ranjan, 2012; Kokulan et al., 2019a).
50 However, they are also important pathways for dissolved and particulate nutrients (Kladivko et
51 al., 1999; Tomer et al., 2015). It has been estimated that 14% of farmlands in Canada (ICID,
52 2018) and 45% of fields in Southern Ontario, Canada (ICID, 2018; Kokulan, 2019) are drained
53 by tile systems. In Alberta, tile drains have also been used to address salinity issues (Broughton
54 and Jutras, 2013). Given their importance in hydrological budgets and biogeochemical transport,
55 there is a need to understand the controlling mechanisms of water and nutrient export from tile
56 systems as an integral part of the broader, modified hydrological system. The ability to integrate
57 a dynamic quantification of tile drainage from fields in hydrological models can help understand
58 the relative importance of this human-induced process as it interplays with an array of other
59 phenomena, including energy and physical mass balance hydrological processes, climate change,
60 and the impacts of modified land management practices on runoff and nutrient export.

61 There are several models that can represent tile drainage at the small basin scale, such as
62 HYPE (Lindstrom et al., 2010; Arheimer et al., 2015), DRAINMOD (Skaggs, 1978, 1980a;
63 Skaggs et al., 2012), MIKE SHE (Refsgaard and Storm, 1995) and SWAT (Arnold et al., 1998;
64 Koch et al., 2013; Du et al., 2005; Du et al., 2006; Green et al., 2006; Kiesel et al., 2010). These
65 models include conceptual components for many key hydrological processes, but research shows
66 that they have been primarily designed and tested for temperate regions (Costa et al., 2020a). In
67 Canada and other cold regions, some unique hydrological processes such as frozen soil,

68 snowmelt, rain on snow, and runoff over and infiltration into frozen or partially-frozen soils may
69 be very important (Rahman et al., 2014; Cordeiro et al., 2017; Pomeroy et al., 1998, 2007; Fang
70 et al., 2010, 2013). Many hydrological processes, such as the sublimation of snow, energy
71 balance snowmelt, and infiltration into frozen soils, are strongly affected by temperature and the
72 phase changes of water, which make many existing models developed for warm regions less
73 appropriate for regions with cold seasons (Pomeroy et al., 2007; Pomeroy et al., 2013; Pomeroy
74 et al., 2016; Fang et al., 2010, 2013). Even for temperate regions, the representation of cold
75 season processes is often underrepresented in models (Costa et al., 2020a).

76 Since the use of tile drainage is becoming popular in many cold regions, it has become
77 important to integrate such human-induced process in specialized hydrological modelling tools
78 for these regions, such as the Cold Regions Hydrological Modelling platform (CRHM, Pomeroy
79 et al., 2007; 2013; 2022). CRHM was initially developed in 1998 to assemble and explore the
80 hydrological understanding developed from a series of research basins spanning Canada and
81 elsewhere into a flexible, modular, object-oriented, multiphysics platform for simulating
82 hydrological processes and basin response in cold regions (Pomeroy et al., 2007; 2022). The
83 modular CRHM platform allows for multiple representations of forcing data interpolation and
84 extrapolation, hydrological model spatial and physical process structure and parameter values.
85 Many existing models typically operate at default daily or monthly time intervals, which is
86 inadequate for the prediction of many short-duration “flashy” hydraulic responses often observed
87 in tiles (Puer et al., 2020; Vivekananthan, 2019; Vivekananthan et al., 2019; Lam et al., 2016a,
88 2016b; Macrae et al., 2019). Indeed, the ability to simulate shorter time intervals (e.g., hourly)
89 facilitates the ability to capture both the rising and falling limbs of tile flow hydrographs, as well

90 as the magnitude of peak flows, both of which are important to tile drain chemistry and export
91 (Rozemeijer et al., 2016; Williams et al., 2015, 2016; Macrae et al., 2019).

92 Hydrological process models such as DRAINMOD, MIKE SHE and SWAT use a
93 combination of empirical and physically based formulations for the simulation of tile flow
94 derived by Hooghoudt (1940), Kirkham (1957), van Schilfgaarde (1974), Bouwer and van
95 Schilfgaarde (1963) and Skaggs et al., (1978). Such formulations contemplate both cases where
96 the water table is below and above the ground surface (Kirkham, 1957). In contrast, simulations
97 of tile drainage in other models such as HYPE use empirically derived recession curves
98 (Eckersten et al., 1994) to simulate tile flow and soil hydrological storage (typically represented
99 as water table). In cases where there is a need for more focus on soil matrix hydrology and less
100 need for understanding hydrological processes at the catchment scale and the relative
101 contribution of tiles (and its interplay), modellers tend to use specialised porous-media PDE-
102 based (partial differential equation-based) numerical models such as HYDRUS (Simunek et al.,
103 2011) and MACRO (Larsbo and Jarvis, 2003).

104 The amount of water transported by tiles depends on soil moisture dynamics and the
105 positioning of the water table, which are in turn affected by many factors, including soil type,
106 surface topography and morphology, as well as the local climate and the hydrological
107 characteristics of the field (Frey et al. 2016; Klaiber et al., 2020; Coelho et al., 2012; King et al.,
108 2015). Thus, to provide reliable estimations of water loss from farmland via surface runoff and
109 tile flow, models must be able to predict soil moisture storage and the water table position
110 accurately (Brockley, 1976; Rozemeijer et al., 2016; Javani-Jouni et al., 2018). Many studies
111 have shown that in some soil types, including silty loam and clay loam soils, the drainable water
112 is less than expected based on the effective porosity (*e.g.*, Skeggs et al., 1978; Raats and

113 Gardner, 1974). Raats and Gardner (1974) have argued that the calculation of drainable porosity
114 requires knowledge of water table position and the distribution of soil moisture above the water
115 table. Skaggs et al. (1978) added that the calculation of drainable porosity should take into
116 account “the unsaturated zone drained to equilibrium with the water table”. However, because
117 the soil column is often composed of different soil layers with varying physical characteristics,
118 drainable porosity varies with evapotranspiration rate, soil water dynamics and the depth of
119 saturated water (Logsdon et al., 2010; Moriasi et al., 2013). In a sandy loam soil, Lam et al.
120 (2016a, 2016b) demonstrated that tile drainage was not initiated until soil was at or above field
121 capacity. Williams et al. (2019) observed in the American Midwest that tile drainage was not
122 initiated until the field storage capacity had been exceeded. It has also been shown that despite
123 the presence of tile drains, the soil above the tile may not always drain all gravitational water
124 following a rainfall/snowmelt event and the soil may remain at or above field capacity (Skaggs et
125 al., 1978; Lam et al., 2016a). Therefore, the soil drainable water content may be considerably
126 smaller than the storage capacity. This is related to matric potential within the vadose zone,
127 which is driven by the soil characteristics but can also be due to the development of a capillary
128 fringe that reduces the rate of vertical percolation through the unsaturated zone, reducing tile
129 flow (Youngs, 2012). Despite this evidence, some saturated flow models that simulate tile flow
130 overlook the effect of capillary rise and over-estimate the soil drainable water. Other models that
131 represent unsaturated flow (i.e., HYDRUS 3D, Simunek et al., 2011) using Richard’s Equation
132 (Richards, 1931) capture the effect of capillary rise and saturation-pressure variation within the
133 soil profile and assess the soil drainable water more accurately. Although the effect of capillary
134 rise is considered in DRAINMOD through the concept of drainable porosity (represented as a
135 “water yield”) (Skaggs, 1980b), and is calculated for layered soil profiles (Badr,1978), it requires

136 detailed information surrounding the soil water characteristic curve (Skaggs, 1980b). Although it
137 is indeed optimal to use soil-specific water characteristic curves, Twarakawi et al. (2009) found
138 that it was possible to employ average representative values from the soil water characteristic
139 curve to represent soil drainable water where a soil-specific curve was not available. They found
140 in this case that the model performance was reduced.

141 In this study, a new tile drainage module was developed and incorporated within the
142 physically based, modular Cold Regions Hydrological Modelling (CRHM) platform (Pomeroy et
143 al., 2022) to enable hydrological simulations in tile-drained farm fields in cold agricultural
144 regions. As a first iteration, the new module was developed for a field with sloping ground and
145 loam soil with imperfect drainage. Such landscapes are common in the Great Lakes Region (e.g.
146 Michigan and Vermont, USA and Ontario, Canada) and tile drainage in such landscapes has not
147 been as widely studied as it has been in clay-dominated soil. In this module, considerations were
148 explicitly included for the effects of capillary rise and annual groundwater water table
149 fluctuations on drainable soil water storage. The use of field capacity and groundwater/soil water
150 elevation head (Twarakawi et al., 2009) to modulate soil drainable water across the soil profile,
151 including the capillary fringe region, is an innovative aspect of the model that has been
152 demonstrated to circumvent the need for water characteristic curves. The development of this
153 physically based module provides insight into hydrological processes in tile drainage from
154 sloping landscapes with imperfect drainage, which are increasingly being artificially drained.

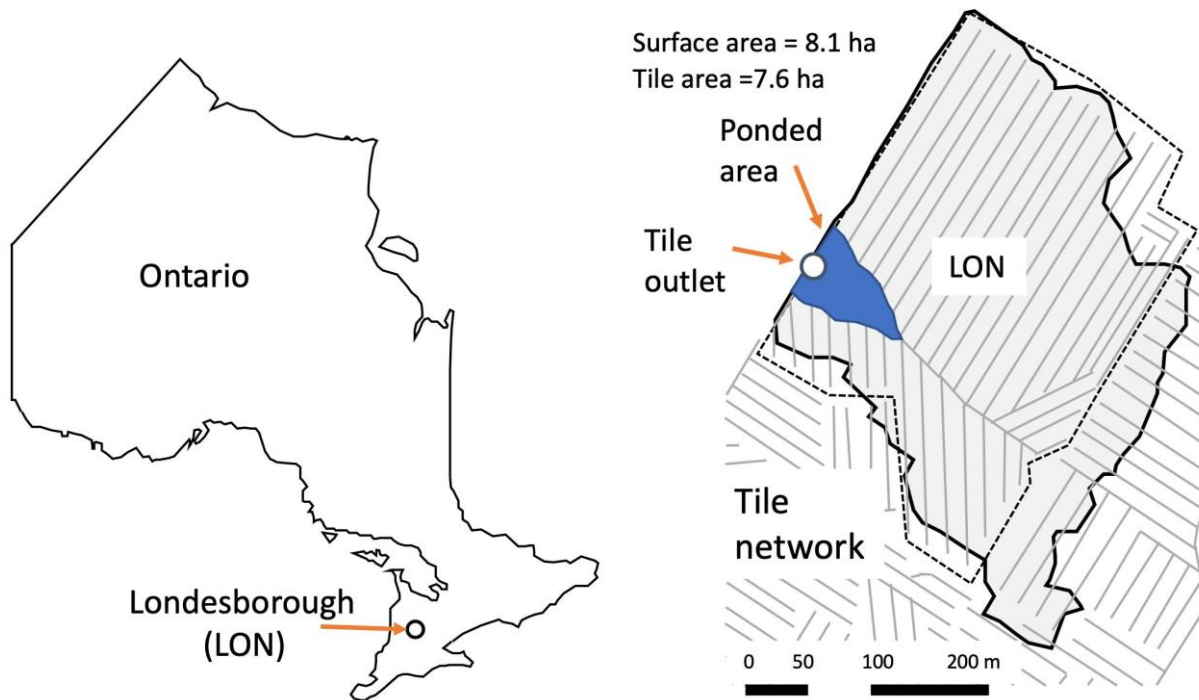
155

156 2. Materials and Methods

157 2.1 Study area

158 The study site is a ~10 ha farm field located near Londesborough, Ontario at UTM 17T 466689m
159 E, 4832203m N, shown as LON in Fig. 1a. Mean annual precipitation recorded in this region is
160 1247 mm (ECCC, 2020). Mean air temperature is 7.2 °C, with annual maxima in July (25.9 °C)
161 and minima in January (-10.2 °C), (ECCC, 2020). Soil texture has been identified as Perth clay
162 loam (Gr. Br. Luvisolic), with a slope between 0.2 and 3.5%. The field is systematically drained
163 with a tile depth of 0.9 m and a spacing of 14 m (laterals). The tile network collects infiltrated
164 water from about 75% of the field (~ 7.6 ha) but may also receive lateral groundwater flow from
165 neighbouring fields. Water yields from the tile drain laterals (10 cm diameter) are discharged via
166 a common tile outlet (main, 15 cm diameter) below ground. Surface runoff from the field is
167 directed toward a common outlet on the surface using plywood berms installed along the field
168 edge (see van Esbroeck et al., 2016). The tile and surface runoff outlets do not join into a
169 common outlet and are fully separated from one another, even during surface ponding events.
170 The field is a corn-soy-winter wheat rotation with cover drops and rotational conservation till
171 (shallow vertical tillage every three years). Additional details related to farming practices are
172 provided in Plach et al. (2019), soil characteristics are provided in Plach et al. (2018a) and Plach
173 et al. (2018b) and equipment and monitoring are provided in van Esbroeck et al., (2016). The
174 outlets for both surface and tile flow are located at the edge of the field and drain into an adjacent
175 field (Fig. 1b). Water tends to accumulate in a topographic low in the field, in front of the field
176 outlet during snowmelt or high-intensity rainfall events, presumably due to either surface runoff
177 or return flow (see ponded area, Fig. 1b). However, surface water or elevated soil moisture
178 conditions are not observed in this topographic low during smaller events or dry periods of the

179 year, suggesting that this saturated ponding is not in a perennial groundwater discharge zone.
180 Although surface ponding is observed in the topographic depression within the field, water
181 discharges freely at the opposite end of the culvert, facilitating the measurement of flow.
182



183
184 a)
185 b) Figure 1. (a) Location of the study area in South of Ontario and the (b) Londesborough (LON) farm with its tile network.
186
187

188 2.2 CRHM: The modelling platform

189 The modular CRHM platform includes options for empirical and physically based calculations of
190 precipitation phase, snow redistribution by wind, snow interception, sublimation, sub-canopy
191 radiation, snowmelt, infiltration into frozen and unfrozen soils, hillslope water movement, actual
192 evapotranspiration, wetland fill and spill, soil water movement, groundwater flow and

193 streamflow (Pomeroy et al., 2007; 2022). Where appropriate, it calculates runoff from rainfall
194 and snowmelt as generated by infiltration excess and/or saturated overland flow, flow over
195 partially frozen soils, detention flow, shallow subsurface flow, preferential flow through
196 macropores and groundwater flow. Water quality can also be simulated (Costa et al., 2021).
197 Modules of a CRHM model can be customized to basin setup, such as delineating and
198 discretizing the basin, conditioning observations for extrapolation and interpolation in the basin,
199 or are process-support algorithms such as for estimating longwave radiation, complex terrain
200 wind flow, or albedo dynamics, but most modules commonly address hydrological processes
201 such as evapotranspiration, infiltration, snowmelt, and streamflow discharge. CRHM discretizes
202 basins into hydrological response units (HRU) for mass and energy balance calculations, each
203 with unique process representations, parameters, and position along flow pathways in the basin.
204 HRU are connected by blowing snow, surface, subsurface and groundwater flow and together
205 generate streamflow which is routed to the basin outlet. The size of TDM HRUs is flexible and
206 can be as small as the size of a single tile pipe (e.g., 1 m) times the pipe spacing (which was 14
207 m in our case study region), and as large as entire tile networks within a given farm or study
208 area. CRHM does not require a stream within a modelled basin. The feature allows CRHM to
209 model the hydrology of cold regions dominated by storage and episodic runoff, such as
210 agricultural fields.

211 Although CRHM has the capability to represent many hydrological and thermodynamic
212 processes, not all processes need/must be represented in all situations. The modular design of the
213 CRHM platform enables the user to activate or inactive specific processes to optimize the model
214 for a particular situation. This is a modelling approach that enables testing different modelling
215 hypotheses and has been pioneered by CRHM and other models, which has inspired a range of

216 hydrological (e.g., SUMMA, Clark et al., 2015a, 2015b), hydrodynamic (e.g., mizuRoute,
217 Mizukami et al., 2015) and biogeochemical (e.g., OpenWQ, Costa et al., 2023a, 2023b)
218 modelling tools. For example, in the current study, blowing snow was not employed in CRHM as
219 it does not appear to be significant at the study site (periodic snow surveys showed relatively
220 uniform snow cover). Preferential flow into tile drains was not developed for the current
221 simulation as although it is a key process in heavy clay soil, as it does not appear to be a
222 significant driver of preferential flow into tile drains in coarse textured soil (Pluer et al., 2020;
223 Macrae et al., 2019). Freeze-thaw processes in soil were also not employed here as there is very
224 little seasonal soil frost in the temperate Great Lakes region due to the persistent snow cover, and
225 where soil frost occurs, it is restricted to brief periods and shallow depths (above 10 cm depth)
226 (Macrae unpublished data).

227

228 2.3 *Observations and input data for the model*

229 Tile flow, water table position (water table elevation head) and surface flow were measured at
230 the site between Oct. 2011 and Sept. 2018 at 15-minute intervals. It was not possible to install
231 more than one measuring station for water table position and soil moisture at the site due to
232 farming activity; consequently, water table elevation head and soil moisture were measured at
233 the approximate midpoint of the field at the edge-of-field. Both tile flow rates and surface runoff
234 were determined using simultaneous measurements of flow velocity and water depths in each of
235 the pipes at the edge-of-field using Hach Flo-tote sensors and an FL900 data logger (Onset Ltd.)
236 (Table A1, Appendix A). Continuous measurements of velocity were included due to the
237 potential for impeded drainage under very wet conditions or caused by the accumulation of snow
238 and ice around the surface culvert in winter. An additional barometrically-corrected pressure

239 transducer (U20, Onset Ltd.) (Table A1) was also used for periods when the flow sensors did not
240 function using a rating curve developed from the depth-velocity sensors. The water table position
241 was measured using a baro-corrected pressure transducer (U20, Onset Ltd.).

242 Air temperature, wind speed, air relative humidity, incoming solar irradiance and rainfall
243 were also measured at the site at 15-minute intervals and used to force the model. Variable
244 names and their symbols in CRHM are listed in Appendix B. The air temperature, wind speed
245 and incoming solar radiance measurements were collected 1 m above ground using a
246 Temperature Smart Sensor S-THB-M002, Wind Smart Sensor Set S-WSET-M002 and a Solar
247 Radiation Sensor (Table A1). Rainfall and relative humidity were measured via a tipping bucket
248 rain gauge (Table A1) and an RH Smart Sensor (Table A1). These observations were
249 continuously recorded throughout the study period, except for brief periods of instrument failure
250 and maintenance, when data from nearby stations (Table T1, Supplementary Material) was
251 substituted using the double mass analysis method (Searcy and Hardison, 1960).

252 Although rainfall was recorded continuously at the field site, snowfall data was not.
253 Snowfall data was obtained from nearby stations (Wroxeter-Davis and Wroxeter, Environment
254 Canada, 2021), located 31.7 km from the field site. Periodic snow surveys done at the site
255 throughout the study period found that data from the nearby stations was a close approximation
256 of snow at the field site (Plach et al., 2019). Hourly snowfall observations from Wroxeter-
257 Geonor were used for the period between 2015 and 2018, whereas daily data from the Wroxeter-
258 Geonor were used for the 2011 to 2014 period, reconstructed to hourly snowfall time series
259 based on the method presented by Waichler and Wigmosta (2003).

260

261 2.4 *Development of the new tile module*

262 A Tile Drainage Module (TDM) was developed within CRHM with the goal of adding the ability
263 to simulate tile flow and the resulting saturated storages (water table) at an hourly time scale.
264 CRHM was forced with hourly precipitation, air temperature, solar radiation, wind speed and
265 relative humidity to calculate hydrological states and fluxes in HRUs and the basin. The model
266 requires parameterizations that specify the hydraulic and hydrological properties of the soil,
267 including its thickness, saturated hydraulic conductivity (K), and surface cover. CRHM
268 calculates water storage and fluxes between HRUs, as well as vertical fluxes amongst different
269 hydrological compartments (within each HRU) that include snow, depressional storage, different
270 soil layers, and groundwater.

271 Using the simulation of soil moisture performed by the original CRHM “*Soil*” module,
272 TDM calculates the dynamic tile flow rate that, in turn, feeds back to soil moisture at each time
273 step. The presence of a capillary fringe (sometimes referred to as the tension-saturated zone
274 within the soil profile) and its effects are considered by limiting the amount of drainable soil
275 water. TDM uses site-specific information regarding the tile network, such as tile depth, diameter
276 and spacing. Information regarding site-specific details regarding tile depth, diameter and
277 spacing may be obtained directly from landowners or can be estimated based on standard design
278 and installation guidelines for the region. This information was used to set up the model together
279 with parameterization to translate the hydrological effects of the soil capillary fringe (CF), if
280 present, through two state variables, CF thickness and CF drainable water (discussed in Section
281 2.5). These two state variables are used to limit the fraction of the soil moisture that can freely
282 drain to the tiles.

283

284 2.4.1 *Soil moisture and water table position*

285 The TDM uses the water quality soil module or soil module (*WQ_soil* or *Soil*), which divides the
286 soil column into two layers: a recharge layer where evapotranspiration and root uptake generally
287 take place and a deeper layer that connects to the groundwater system. Since CRHM's state
288 variable for soil moisture is soil water storage volume (Fig. 2a), the model results were converted
289 into water level elevation above the semi-permeable layer (Table B1, Appendix B; see Fig. 2b
290 for comparison with water table observations) by dividing volumetric soil moisture content
291 (Table B1) by soil porosity (Table B1) for the cases with no capillary fringe above the water
292 table. Additional steps were taken for periods when a capillary fringe developed (discussed
293 below).

294

295 2.4.2 *Capillary fringe and drainable water*

296 Soil moisture in the capillary fringe is equal to the field capacity (θ_{fc}) (Bleam, 2017, Sect. 2.4).

297 Therefore, while the positioning of the capillary fringe responds dynamically to the matric
298 potential, the saturation profile within the capillary fringe remains constant, as well as its
299 thickness because it only depends on the pressure head (capillary forces) that are related to the
300 grain size distribution and field capacity (h_{fc}) as introduced by Twarakawi et al. (2009).

301 Therefore, the drainable water in the capillary fringe becomes the difference between saturation
302 (θ_s), computed dynamically in CRHM, and θ_{fc} , which corresponds to the water held by capillary
303 forces at field capacity (Fig. 2). Accordingly, Fig. 2 shows the schematic soil characteristic curve
304 for the three water level conditions contemplated in the model.

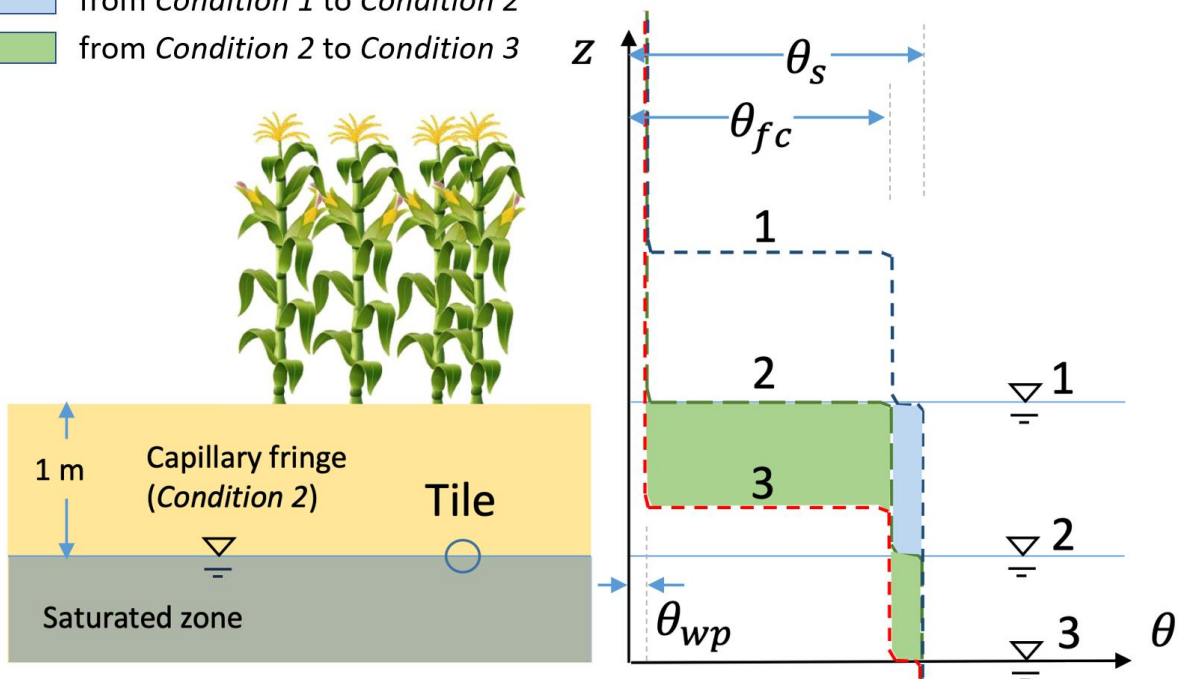
305 1. *Condition 1* is when the matric head is at the surface and the soil is completely saturated;

- 306 2. *Condition 2* is when the matric head drops but the upper boundary of the capillary fringe
 307 is at the soil surface; and
- 308 3. *Condition 3* is when the water table drops further and the upper boundary of the capillary
 309 fringe drops beneath the surface.

310 In essence, the soil is completely saturated (θ_s) in *Condition 1*. Between *Conditions 1* and 2, the
 311 capillary fringe occupies the entire soil column above the water level; thus, it can only release
 312 the volume of water corresponding to $\theta_s - \theta_{fc}$ or φ_c (dimensionless). Between *Conditions 2* and 3,
 313 two layers with distinct hydraulic characteristics develop: (1) the top one at θ_{wp} that releases
 314 water up to $\theta_{fc} - \theta_{wp}$, and (2) the lower one that corresponds to the capillary fringe and can
 315 release up to the volume of water corresponding to $\theta_s - \theta_{fc}$ or φ_c .

Drained water when the water table position is changed:

- from *Condition 1* to *Condition 2*
- from *Condition 2* to *Condition 3*



316
 317 Figure 2. Schematic representation of the capillary fringe above the water table assuming a 1-m thickness (for demonstration
 318 purposes). The soil characteristic curves are shown for the three water level conditions considered: water level at the (1) surface,

319 (2) intermediate depth, and (3) deeper depth. Two transitional drops can be seen in the characteristic curves, one from saturation
320 (θ_s) to field capacity (θ_{fc}) (between *Conditions 1* and 2) and one from field capacity to wilting point (θ_{wp}) (between *Conditions*
321 2 and 3). The coloured areas (green and blue) of the right panel correspond to the amount of water that can be released between
322 *Conditions 1* and 2 (blue) and between *Conditions 2* and 3 (green).

323

324

325 2.4.3 *Tile flow calculation*

326 A modified version of the Hooghoudt equation was used to calculate tile flow (Smedema et al.,
327 2004), which presumes no surface ponding, an assumption that generally holds at the study site
328 (Eq. 1), where water ponds only during very wet periods and on a small portion of the study site
329 (see Fig. 1b). Hooghoudt's equation (Hooghoudt, 1940) is a steady state, physically based
330 equation for saturated flow toward the tile drain. Flow estimates are provided based on the
331 hydraulic conductivity of the soil and matric potential. It allows different saturated hydraulic
332 conductivities for the layers above (AL) and below (BL) the tile (Fig. S1). In the particular case
333 of the case study site, soil surveys have reported almost the same soil type (Loam) down to the
334 depth of 90 cm (e.g., Van Esbroeck et al., 2016; Plach et al., 2018b), which was parameterized in
335 the model set up as,

336

$$337 \quad q = \frac{8 \times K_2 \times d \times h}{L^2} + \frac{4 \times K_1 \times h^2}{L^2}, \quad (1)$$

338

339 where K_1 and K_2 are respectively the saturated hydraulic conductivity in the upper and lower
340 layers in mm h^{-1} ; L is the tile spacing in mm; h is the water table elevation above the tile in mm,
341 d is the lower layer thickness in mm (Fig. S1), and q is the predicted tile flow in mm h^{-1} . The

342 only variable that is dynamically updated by CRHM is h . Equation (1) is used to estimate the tile
 343 flow.

344

345 2.4.4 Calculation of the effect of tile flow on soil moisture and water levels

346 The simulated tile flows (see Sect. 2.3.3) are subtracted from the soil moisture. To calculate
 347 saturated storage (water table or groundwater elevation head level) from soil moisture calculated
 348 by the model, a threshold soil moisture content (sm_t) is defined, which consists of drainable
 349 water in the soil when the upper boundary of the capillary fringe is at the surface (*Condition 2*,
 350 Fig. 2) and was calculated as:

351

$$352 \quad sm_t = sm_{max} - (C_t \times \varphi_c) \quad , \quad (2)$$

353

354 where sm_{max} is the maximum soil moisture and C_t is the capillary fringe thickness in mm.

355 However, since the hydrological conditions of the soil are markedly different between the two
 356 transitional situations described in Sect. 2.3.2 and Fig. 2 (*Condition 1 to 2* and *Condition 2 to 3*),
 357 a step function was deployed for determination of the matric potential:

358

$$359 \quad WT = \begin{cases} \frac{sm_t - (C_t \times ((\varphi_s - \varphi_c) + \theta_{wp}))}{\varphi_s + \theta_{wp}} + \frac{sm - sm_t}{\varphi_c} & , \text{if between Conditions 1 and 2} \\ \frac{sm_{max}}{\varphi_s + \theta_{wp}} - \left(\left(\frac{sm_t - sm}{\varphi_s} \right) + C_t \right) & , \text{if between Conditions 2 and 3} \end{cases} \quad (3)$$

360

361 where WT is water table elevation (or soil saturated storage, SSS) in mm from the bottom of the
 362 soil, and sm is soil moisture (both saturated and unsaturated storage) in the given time step in

363 mm. Equation (3) is determined based on soil moisture curves in Fig. 2 and water level
364 *Conditions 1-3* discussed in Sect. 2.3.2. In Fig. 2, the first and second parts of Eq. (3), which
365 refer to *Conditions 1* to 2 and 2 to 3, respectively, correspond to the volumes of soil water
366 highlighted in “blue” and “green.”

367

368 2.4.5 *Lower semi-permeable soil layer and periodicity in annual groundwater levels*

369 This model application focused on the study site field without including other adjacent areas.

370 This was possible because years of field monitoring at this site have demonstrated that there is no
371 observable surface flow into the site from adjacent farms. The tile network is restricted to the
372 field and is not connected to tile drains or surface inlets in adjacent fields. However, field soil
373 water table observations show evidence of annual groundwater level periodicity/fluctuation (Rust
374 et al., 2019) that are sinusoidal in nature and cannot be neglected. Some studies predict the
375 annual groundwater oscillations or the annual responses of groundwater to precipitation by using
376 sine and cosine functions (De Ridder et al., 1974; Malzone et al., 2016; Qi et al., 2018). De
377 Ridder et al. (1974) studied the design of the drainage systems and described the seasonal
378 groundwater fluctuations observed in wells using sinusoidal curves. Malzone et al. (2016) used a
379 sine function to predict annual groundwater fluctuations in the hyporheic zone. Qi et al. (2018)
380 and Rust et al (2019) used a cross-wavelet transform, consisting of the superposition of sine and
381 cosine curves, to predict shallow groundwater response to precipitation at the basin scale. This
382 approach was used in this application to simulate annual fluctuations in groundwater water
383 tables, in Eq. (4), with a period of 1 year, minimums around the middle of the growing season
384 (mid-July), and maximums in the cold season (early February). This translates into the lowering
385 of the matric potential during the growing season, causing soil water seepage, and an elevated

386 matric potential during the non-growing season, causing an increase in the soil moisture
387 consistent with field observations. Thus, a sine function representing the annual fluctuations in
388 groundwater water table ($G_{y,i}$) is defined as below:

$$390 \quad G_{y,i} = \left[A \times \sin \left(\frac{(T_s - D_d \times 24) \times 360}{24 \times 365.25} \right) - B \right] \times f_{y,i} \quad (4)$$

391
392 where T_s is the time step number, D_d is a time delay in days, A is the amplitude of the soil water
393 table (WT/SSS) fluctuation, and B is an intercept factor. $f_{y,i}$ is a seasonal factor. The sine
394 function coefficient (D_d , A , and B) and seasonal factor were adjusted for the whole period and
395 for each year through model verification and shown in Table 1. Appendix C provides more
396 details on the implementation of Eq. (4).

397

398 2.5 Model application and multi-variable, multi-metric validation

399 The study site is a relatively small field, and 2 HRUs were sufficient to capture its hydrological
400 dynamic in CRHM. The HRUs represent (1) the area immediately upstream of the outlet where
401 surface ponding occurs (depression storage); and (2) the remaining field (Fig. 3). The maximum
402 ponding capacity of HRU 1 was estimated using the spatially distributed hydrodynamic model
403 FLUXOS-OVERFLOW (Costa et al., 2016, 2020b). The CRHM model and new TDM module
404 were set up using the information described in Table 1. Soil textures at the LON site measured in
405 a 25m grid across three soil depths (0-25 cm, 25-50 cm, and 50-100 cm) averaged 29% sand,
406 48% silt, and 23% clay (Ontario Ministry of Agriculture, Food and Rural Affairs Soil Team,
407 unpublished data). This soil grain size distribution corresponds with a soil-saturated hydraulic
408 conductivity of $\sim 0.56 \text{ cm h}^{-1}$ ($\sim 10^{-2.5}$) (Garcia-Gutierrez et al., 2018), which was implemented

409 in CRHM (0.5 cm h^{-1}), corresponding to a field capacity of 0.03 and h_{fc} of $\sim 0.8 \text{ m}$ (Twarskawi
410 et al., 2009, based on a drainage flux of 0.1 cm d^{-1}).

411

412 A robust multi-variable, multi-metric model evaluation strategy was deployed to verify the
413 capacity of the model to predict tile flow and its impact on the local hydrology. The state
414 variables examined were tile flow, surface flow, and matric potential. The multi-metric approach
415 contemplated five different methods, namely the Nash-Sutcliffe efficiency (*NSE*), Root-Mean-
416 Square Error (RMSE), Model Bias (Bias), Percentage Bias (PBias), and RMSE-observation
417 standard deviation ratio (RSR). See Appendix C for more details about the methodology used. It
418 is generally assumed that $NSE > 0.50$, $RSR \leq 0.70$, and *PBias* in the range of $\pm 25\%$ are
419 satisfactory for hydrological applications (Moriassi et al., 2007). Hourly values were used in these
420 calculations, which departs from the daily and monthly analyses typically reported for these
421 types of models. Although this is a challenging proposition, it is an important one as it
422 constitutes a necessary step forward toward more detailed, accurate, and advanced models for
423 these regions. For example, Costa et al., (2021) noted that the successful extension of
424 hydrological models to water quality studies relies on their ability to operate at small time scales
425 in order to capture intense, short-duration storms that may have a disproportional impact on the
426 runoff transport of some chemical species such as phosphorus – in essence, to capture hot spots
427 and hot moments for flux generation.

428

429

430 Table 1. Key model parameters in CRHM for representation of the LON site.

431

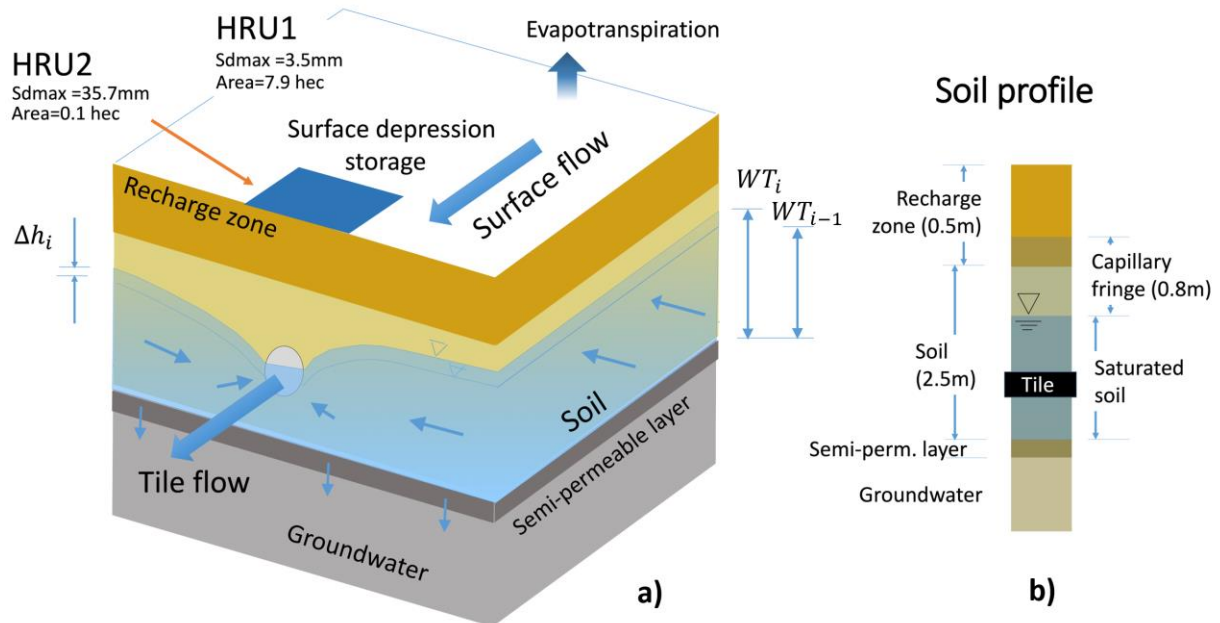
Model Parameter	Value	Unit	Source	Adjusted/Calibrated	Comment
Soil depth	2	m		No	Assumed
Semipermeable layer depth	3	m		No	Assumed
Tile depth	0.9	m		No	Farmer/Blueprints of the field
Corn root depth	0.5	m		No	Online sources
Soil recharge zone thickness	0.5	m		No	Based on the root depth
Tile spacing	14	m		No	Farmer/Blueprints of the field
Soil porosity (soil drainable water) φ_s	0.045			Yes	Adjusted
K in below layer	5	mm h ⁻¹		Yes	Adjusted
K in above layer	5	mm h ⁻¹		Yes	Adjusted
Capillary fringe thickness	0.8	m		Yes	Adjusted
Capillary fringe drainable water φ_c	0.03			Yes	Adjusted
Surface depression in small area close to farm surface flow outlet (HRU2)	35	mm		Yes	Calculated
Surface depression in rest of the area (HRU1)	0	mm		No	Calculated
Surface area of HRU1	79000	m ²		No	Field observations and DEM
Surface area of HRU2	1000	m ²		No	Field observation and DEM
Soil module name in CRHM	WQ_soil			No	
Infiltration module name in CRHM	GreenAmpt			No	
Soil type in GreenAmpt module	5			Yes	Adjusted
Saturated K in GreenAmpt module	6	mm h ⁻¹		Yes	Adjusted

Soil wilting point	0.025		Yes	Adjusted
A , in sine function	0.025	mm h^{-1}	Yes	Adjusted
B , in sine function	-0.005	mm h^{-1}	Yes	Adjusted
D_d , in sine function	15	d	Yes	Adjusted
$f_{2012,2}$ (Seasonal factor, sine function)	2.0		Yes	Adjusted
$f_{2015,2}$ (Seasonal factor, sine function)	1.8		Yes	Adjusted
$f_{2016,2}$ (Seasonal factor, sine function)	2		Yes	Adjusted
$f_{2017,2}$ (Seasonal factor, sine function)	1.4		Yes	Adjusted
$f_{y,i}$	1		No	By default for $y =$ 2012 to 2017 and $i = 1, 2$

432

433

434



435

436 Figure 3. a) Schematic conceptual view of the CRHM model configuration, including soil layers, water table (WT/SSS),

437 groundwater, and tile flow.; and b) soil profile, including the capillary fringe and its location relative to the soil and tile.

438

439 **3. Results**

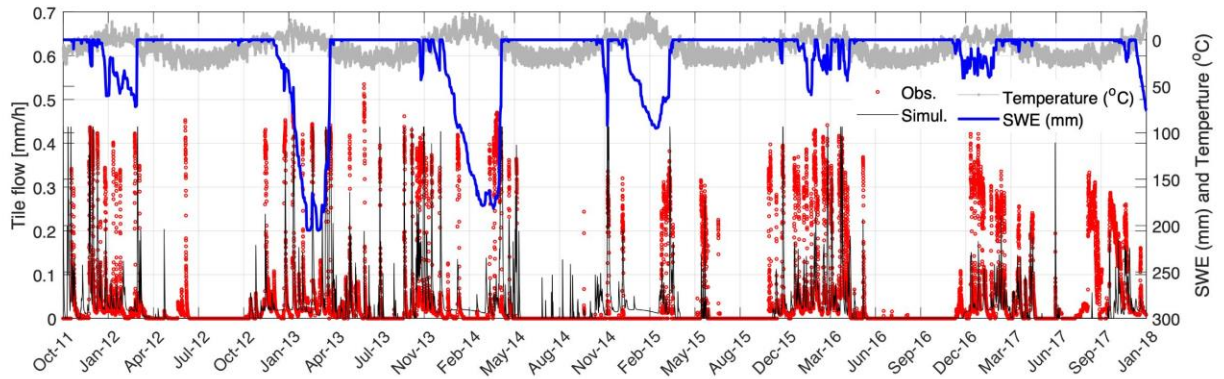
440

441 *3.1 Tile flow*

442 The model was able to capture most tile flow events, both in terms of the timing and magnitude
443 of peak flows and the most important seasonal patterns (Fig. 4). For example, the almost
444 complete absence of tile flow during the growing season (May to September) was captured. The
445 simulated flow peaks generally had a good agreement with observations, as well as the low flow
446 or base flows during cold periods (December-March). The ascending and descending limbs of
447 the response signal were also adequately predicted.

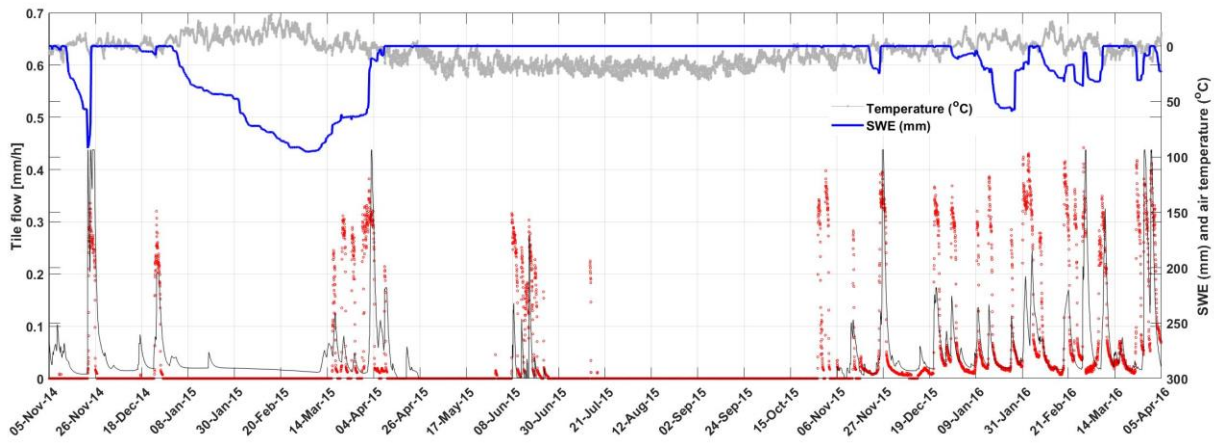
448

449 Results show that tile flows generally occur during snowmelt events, as indicated by the
450 synchrony between snow water equivalent (SWE) depletion and tile flow. The maximum
451 snowpacks (or snow water equivalent, SWE) were markedly smaller during the winters of 2016
452 and 2017 when compared with those of 2013 to 2015. However, this did not necessarily translate
453 into lower tile flows as precipitation also occurred as rain during these seasons. Although the
454 magnitude of tile peaks was not always assessed accurately, the model was able to capture the
455 annual trends of both an absence of tile flow during the summer months (growing season) and
456 the ascending and descending limbs of the tile hydrograph during events (Figure 4).



457

458 a)



459

460 b)

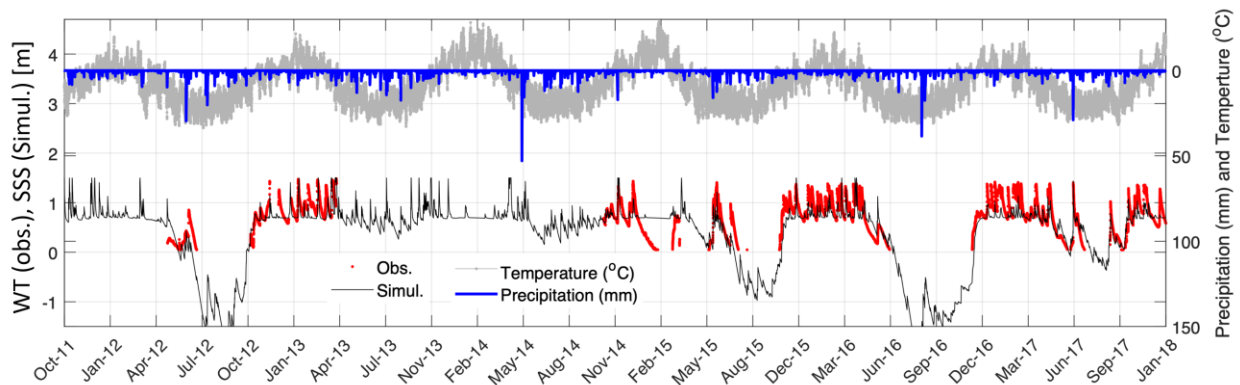
461 Figure 4. Comparison between observed and simulated tile flows, simulated SWE (snow water equivalent), and observed air
 462 temperature in the LON site.

463

464 3.2 Water table or soil saturated storage

465 Simulated soil saturated storage and the observed water table are compared in Fig. 5, alongside
 466 air temperature and precipitation observations. Despite the observation gaps, the model agrees
 467 well with observations. Above tile drains, water table fluctuations are controlled by
 468 infiltration/recharge, tile flow, groundwater flow, and matric potential that affect the drainable
 469 water from the capillary fringe. This causes flashier storage responses above the tile that are

470 captured well by the model. In contrast, tiles do not withdraw water from the soil layer below
 471 the tile pipe and thus do not control water table fluctuations when levels are below the drain pipe,
 472 and tile drains simply do not flow during such periods. During the growing season, both the
 473 observed and simulated water table (or saturated storage) drops abruptly because of the seasonal
 474 lowering of the regional groundwater water table. In the growing seasons of 2012, 2015 and
 475 2016, which were dry years, large declines in the water table and saturated storage were
 476 observed, whereas in wetter years such as 2013 and 2014, seasonal water level declines were
 477 smaller. The seasonal declines in water level during the growing season led to a cessation in tile
 478 flow in most years (Fig. 4, 5), even following rainfall events. For example, there was a large
 479 precipitation event (~35 mm) in the growing season of 2016 that did not produce tile flow
 480 (apparent in both model and observations).

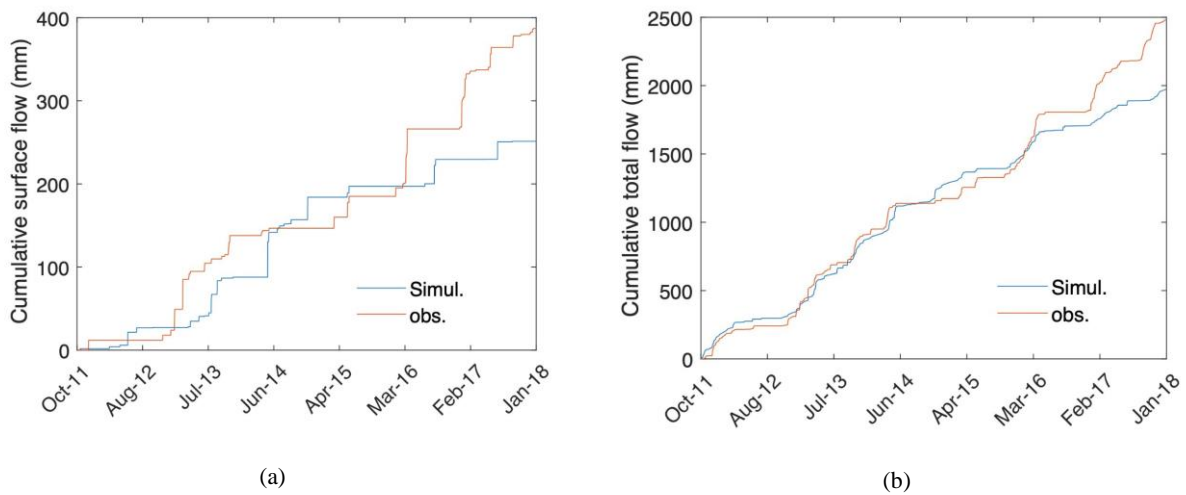


481
 482 Figure 5. Time series of the simulated saturated storage and observed water table (groundwater table) along with the observed
 483 temperature and precipitation. The horizontal line shows the depth of the tile pipe.

484
 485 *3.3 Surface flow and total flow*

486 The model was not always able to capture the observed surface flow as satisfactorily as it
 487 captured tile drainage (Fig. 6a). Some of the possible reasons are uncertainties in the
 488 measurements of surface flow due to ponding in surface depressions on the field, which impeded

489 the drainage of some of the surface runoff prior to when it exited the field through the culvert
 490 (see Fig. 1), or due to uncertainty in field estimates of SWE. However, the model performance
 491 improves considerably when both runoff and tile flow are combined (referred to as total flow,
 492 Fig. 6b). Indeed, most of the flow from the field was through tile drains (80% in 5-year average)
 493 rather than surface runoff (20% in 5-year average, Plach et al., 2019). The underestimation of
 494 both cumulative total and surface flows during 2017 and 2018 is possibly due to the removal of
 495 the blockage in the tile pipe in early 2017, which may have affected both surface and tile flow.



496 Figure 6. Observed and simulated cumulative surface flow (a) and total flow (b) with their performance coefficients.

497

498 3.4 Overall model performance

499 The model performance was calculated based on hourly data for various model outputs (Table
 500 2). The results confirm that the model is robust in the sense that it can capture the main patterns
 501 of tile flow, surface flow, and matric potential levels. The PBias values are below 25% for most
 502 of the fluxes and cumulative fluxes. The RSR values are also generally below 1.0. The NSE
 503 values are positive and above 0.3 for most fluxes, except for surface flow, where the model
 504 exhibited some difficulties.

505

506 Table 2. Performance coefficients for surface flow, tile flow and water table (WT/SSS), as well as total (tile + surface) flow, for
 507 the simulation period of October 2011 to January 2018. The coefficients were calculated for both hourly and daily flow rates.

Performance coefficients	Surface flow	Tile flow	WT (SSS) (m)	Total flow	
NSE*	-2.29	0.31	0.49	-1.38	Coefficients calculated for hourly flow rates (mm h ⁻¹)
RMSE [^]	0.27	0.08	0.26	0.30	
Bias [#]	0.54	0.24	0.14	0.28	
PBias [§]	21.77	17.91	10.46	18.63	
RSR ^{&}	1.82	0.83	0.71	1.54	
NSE	-0.73	0.29	0.50	0.01	Coefficients calculated for daily flow rates (mm d ⁻¹)
RMSE	2.04	1.72	0.24	2.92	
Bias	0.35	0.20	0.09	0.22	
PBias	35.11	19.63	9.33	21.73	
RSR	1.31	0.84	0.70	0.99	

508 *Nash-Sutcliffe efficiency, [^]Root-Mean-Square Error, [#]Model Bias, [§]Percentage Bias, [&]RMSE-observation standard deviation ratio

509

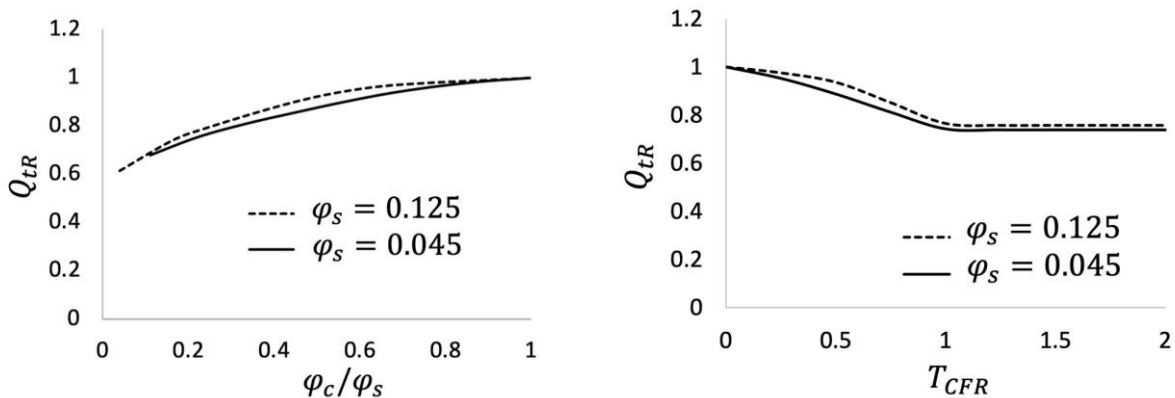
510 3.5 *Presence of capillary fringe: effects and hypotheses*

511 Results show that the thickness and vertical positioning of the capillary fringe have a strong
 512 impact on the amount of drainable soil water that can flow into tiles. To investigate this effect
 513 further, the response of tile flow and soil moisture to changes in the capillary fringe was
 514 investigated. It should be noted that although this thickness may slightly change depending on
 515 the soil type and water retention curves (Skaggs et al., 1978), the model assumed a constant
 516 value given the catchment-scale nature of the simulations and myriad of processes contemplated.
 517 However, despite the simplification, the vertical positioning of the capillary fringe was still
 518 computed and enabled a dynamic (time-dependent) calculation of the drainable soil water that is
 519 available for tile drainage over time.

520

521 *Effect of capillary fringe on tile flow*

522 Figure 7a relates the simulated normalized total cumulative tile flow (Q_{tR} , total tile flow divided
 523 by the total tile flow when there is no influence of capillary fringe) to capillary fringe drainable
 524 water ($\varphi_{CR} = \varphi_c/\varphi_s$) for two different φ_s values (0.045 and 0.125). The values were
 525 normalized for comparison purposes. As expected, the model indicates that tile flow increases
 526 with drainable water, but the relationship is non-linear, likely because as tile carrying capacity is
 527 exceeded more frequently, there is more opportunity for groundwater seepage and
 528 evapotranspiration. The direct effect of φ_s (comparing the solid and dashed lines) on tile flow is
 529 small because the amount of water that can effectively drain to the tile is controlled by the
 530 capillary fringe and the associated drainable soil water. Figure 7b looks at the impact of the
 531 capillary fringe thickness on tile flow. Here, the values are also normalized. Results show that
 532 Q_{tR} decreases with increasing normalized thickness of the capillary fringe, T_{CFR} ($\frac{T_{CF}}{D_t}$, capillary
 533 fringe thickness divided by tile depth), but only while the T_{CFR} is less than 1 that is when the
 534 capillary fringe position is above the tile but has not reached the soil surface. Beyond this point,
 535 increments in the capillary fringe thickness have no impact on tile flow because *Condition 1* has
 536 been reached (see Fig. 2), which essentially means that the capillary fringe has reached the soil
 537 surface.



a)

b)

538 Figure 7. Comparison between normalized tile flow (Q_{tR}) and (a) normalized drainable soil water (φ_c/φ_s) and capillary fringe
539 thickness (T_{CFR}) for different maximum soil saturation values (φ_s), by drawing the model prediction lines.

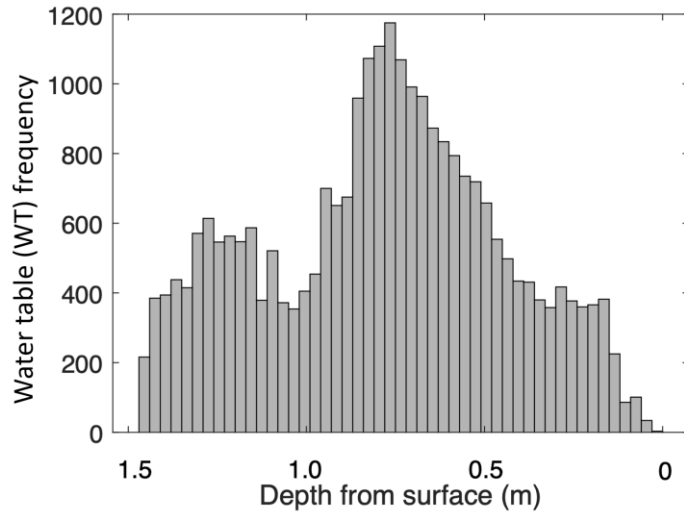
540

541 *Effect of capillary fringe on soil moisture*

542 Observations and model results of WT (or SSS as an indicator of soil moisture) reveal a bimodal
543 frequency distribution (Fig. 8 and 9, respectively) with peaks at 0.85 m and 1.25 m depth, with
544 the former corresponding to the depth of the tile pipe and the second peak reflecting capillary
545 fringe thickness. In the simulated soil saturated storage (SSS/WT) frequency distributions (Fig.
546 9), the first peak highlights again the efficiency of the tile in removing soil moisture. In contrast,
547 the second peak indicates a strong model response to differences in the capillary fringe thickness.
548 It shows that when there is near-constant discharge from the bottom of the soil layer, the matric
549 potential varies the greatest while it remains between the tile depth and the soil surface. While
550 the matric potential fluctuates faster and is more unstable within this range, it also remains there
551 for shorter periods. This bimodal response tends to push the matric potential below the tile.

552

553 The bimodal behavior of the observed water table and simulated saturated storage demonstrated
554 here provides the opportunity to quantify the thickness of the capillary fringe using continuously
555 monitored water table position. The capillary fringe thickness determined using this method can
556 then be used as an input to the TDM module.

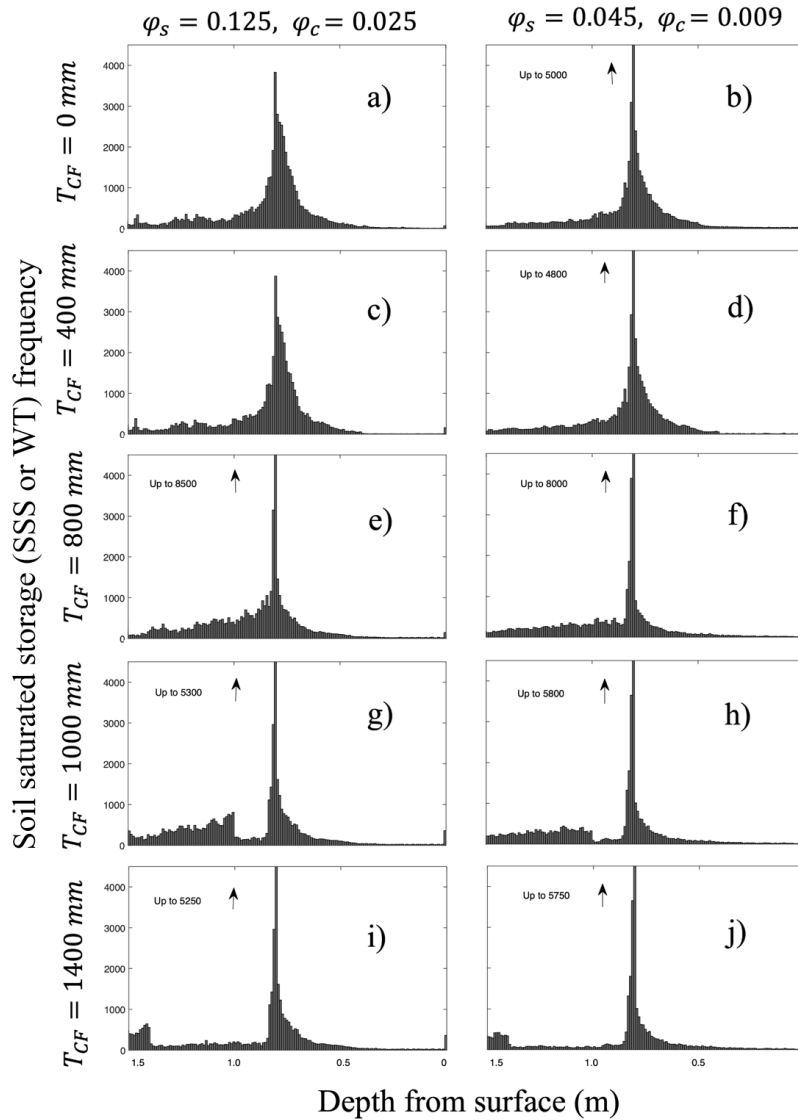


557

558

Figure 8. Histogram of the observed water table distribution for the period pf 2011 to 2018 in LON (Londesborough).

559



560

561

Figure 9. Histograms of the simulated soil saturated storages (SSS or WT) for the capillary fringe thicknesses of 0 (a,b), 400

562

(c,d), 800 (e,f), 1000 (g,h) and 1400 (i, j) mm and for the φ_s and φ_c of 0.125 and 0.025 (left column) as well as 0.045 and 0.009

563

(right column).

564

565 4. Discussion

566

The new TDM module developed for CRHM was able to capture tile drainage flow and its effect

567

on the hydrological patterns of a farm field in southern Ontario. This module helps extend the

568

existing capacity of representing the effect of tile drainage in the hydrology of agricultural cold

569 regions, from the colder Canadian Prairies to the more temperate Great Lakes region. Tile
570 drainage is prevalent across much of the cultivated lands in the Great Lakes basin and adjacent
571 regions from southern Canada to the upper US Midwest. It is expanding in the eastern Canadian
572 Prairies as well. The new TDM module will also permit simulating the impacts of a changing
573 climate on runoff processes in these landscapes. In addition to this potential, the development of
574 the TDM has also provided insights into hydrological processes in tile-drained landscapes. These
575 are discussed in more detail below.

576

577 *4.1 Insights into key control mechanisms of tile flow for catchment-scale simulations*

578 The model suggests that tile flow may not be accurately predicted exclusively based on the
579 matric potential and soil saturated hydraulic conductivity as suggested by the steady-state flow
580 assumptions of the Hooghoudt's equation (Hooghoudt, 1940). Our results indicate two additional
581 controls: (1) the amount of drainable soil water in the soil, which has also been identified in
582 some field studies (*e.g.*, Skaggs et al., 1978; Moriasi et al., 2013) and (2) fluctuations in the
583 groundwater table (GWRD) are equally important to account for in catchment-scale simulations.
584 However, the relationship between drainable water and tile flow rates is non-linear, as
585 demonstrated in Fig. 7a. This is because the residence time for groundwater seepage and
586 evapotranspiration increases when the hydraulic tile carrying capacity is exceeded.
587 Comparatively, the effect of soil drainable water, φ_s (see also Fig. 7a) on tile flow is small
588 because the capillary fringe and associated drainable soil water control the amount of water that
589 can effectively flow to the tile.

590

591 The verification of the model also indicated that the slopes of the rising and falling limbs of tile
592 flow hydrographs and WT were very sensitive to (1) the ratio between K and drainable soil
593 water; and (2) the net outflow in the soil through tile flow and groundwater level fluctuations
594 (GWRD). This is supported by previous studies showing rapid responses of tile flow to
595 precipitation events (Gentry et al., 2007; Smith et al., 2015) and others that have related rapid
596 responses in tile discharge to antecedent moisture conditions (Macrae et al., 2007; Vidon and
597 Cuadra, 2010; Lam et al., 2016a; Macrae et al., 2019), which can be affected by the development
598 of a capillary fringe and its holding capacity.

599

600 Results show that large fluctuations in WT (or SSS) and tile flow during the cold season, when
601 the water table tends to be above the tile, are primarily triggered by the development of a
602 capillary fringe that reduces the amount of drainable soil water. Model sensitivity tests showed
603 that a small amount of drainable soil water produces steeper rising and falling responses (and
604 with larger fluctuation amplitudes) in both the water table (saturated storage) and the tile flow.
605 Indeed, this pattern can be observed by exploring differences in tile drain responses in clay loam
606 soils with larger field capacities (and correspondingly smaller drainable water) and smaller
607 hydraulic conductivity which are more likely to experience pronounced oscillations (*e.g.*, steeper
608 rising and falling response curves) compared to tile drain responses of sandy soil, which is
609 characterized by reduced capillary forces, lower field capacities (but correspondingly larger
610 drainable water) and higher hydraulic conductivity. Notably, both model and observations of
611 WT/SSS (as a proxy for soil moisture) reveal a bimodal (*i.e.*, two peaks) frequency distribution
612 when examined in relation to the tile depth and capillary fringe thickness (Fig. 8 and 9,
613 respectively). The two peaks (*i.e.* most frequently observed WT or SSS conditions) correspond

614 with the (1) depth of the tile pipe (0.75 m), which demonstrates the efficacy of the tile at rapidly
615 removing excess soil water, and the (2) the capillary fringe thickness (for the depths of 1.0 and
616 1.4 m, Figs. g, h, i and j) beyond which the amount of drainable water above the water level
617 significantly increases.

618
619 These findings align well with studies such as Lam et al. (2016a) that recorded soil moisture near
620 saturation after tile flow had ceased, suggesting the development of a capillary fringe. Combined
621 experimental and modeling works, such as in Moriasi et al. (2013) and Logsdon et al. (2010),
622 also discuss the impact of drainable soil water (“drainable porosity” or “specific water yield”) on
623 tile flow and note that the drainable water is, in turn, dependent on the soil type, soil-water
624 dynamic and water table depth. However, these studies did not explore the dynamic nature of the
625 capillary fringe and its thickness relative to the soil column above in determining the transient
626 amount of drainage soil water that will impact the WT distribution and tile flow differently over
627 time (*Conditions 1 to 3*, see Fig. 2). Herein, while a capillary fringe with a fixed thickness that is
628 generally related to the soil properties was assumed, its vertical positioning was simulated
629 dynamically, which allowed determining the drainable soil water based on the evolution of
630 pressure head corresponding to field capacity. Thus, the development of the TDM has provided
631 a step forward in the modeling of tile drainage and suggests that in loam soils such as those at the
632 study site, the effects of a capillary fringe on tile flow should be included. Soil moisture (soil
633 unsaturated storage) measurements from the study site by Van Esbroeck et al., (2017) between
634 November 2011 and May 2014 from depths of 10, 30, and 50 cm (using EC-5 Soil Moisture
635 Smart Sensor) showed that almost 90% of the gravitational soil moisture drains out with 0.5 to
636 2.5 h.

637

638 4.2 *Importance of capturing seasonal patterns in groundwater to improve tile flow*

639 *predictions*

640 The GWRD changed dramatically between seasons affecting soil moisture (both saturated and
641 unsaturated storage of the soil) and tile flow patterns. Both observations and model results show
642 that low precipitation and higher evapotranspiration rates tend to produce little tile flow during
643 the growing season. These seasonal patterns in precipitation and evapotranspiration are
644 accompanied by a reduction in soil moisture (both unsaturated storage and saturated storage)
645 that leads to a substantial storage capacity in fields. Even following moderate and high-intensity
646 storms during the growing season, rapid soil moisture increases are observed (both saturated and
647 unsaturated soil storage); however, tile flow rarely develops, suggesting that the soil is able to
648 hold the water (Lam et al., 2016a; Van Esbroeck et al., 2016). In contrast, tile flow is often
649 observed during the cold season, even during smaller rainfall-runoff and snowmelt events
650 because of reduced soil storage but also a seasonal increase in GWRD (Lam et al., 2016a;
651 Macrae et al., 2007, 2019; Van Esbroeck et al., 2016). This concurs with several studies
652 throughout the Great Lakes and St. Lawrence region that have reported stronger tile responses
653 during the non-growing season, with the summer months often showing little to no tile flow
654 (Lam et al., 2016a, 2016b; Jamieson et al., 2003; Macrae et al., 2007; Hirt et al., 2011; King et
655 al., 2016; Van Esbroeck et al., 2016; Plach et al., 2019).

656

657 These results (the controlling effect of soil drainable water and groundwater level fluctuations on
658 tile flow) suggest that while soil moisture (both SSS and unsaturated storage) is largely
659 controlled by tile flow rather than GWRD in the cold season, this reverses in the growing season

660 (*i.e.*, soil moisture controls tile flow), with soil moisture (both SSS and unsaturated storage)
661 being also impacted by evapotranspiration. The controlling effect of groundwater fluctuations in
662 the growing season has also been studied by Hansen et al., (2019). The model indicated that the
663 rapid drops observed in WT during the growing season could not be explained by
664 evapotranspiration alone as well as the crop root depths, thus pointing to the role of GWRD.
665 Johnsen et al. (1995) and Akis (2016) also showed that the effect of groundwater accretion was
666 more effective on tile flows than surface runoff. Also, Vaughan et al. (1999) found that tile drain
667 flows in their study site in San Joaquin Valley of California were better explained and related to
668 nonlocal groundwater appearance than to local variations in irrigation amount,
669 evapotranspiration, variation in water storage or tile drain blockage.

670

671 **5. Conclusion**

672 A new tile drain module within the modular Cold Regions Hydrological Modelling platform has
673 been created and tested at the field scale to support the management of agricultural basins with
674 seasonal snow covers. The model was tested and validated for a small working farm in southern
675 Ontario, Canada, and presents a step forward in the dynamic simulation of tile flow and its
676 effects on the hydrological cycle in cold climates. Observations and model results showed that
677 the dynamic prediction of tile flow and soil moisture at catchment scales needs to account for (1)
678 the amount of drainable soil water that can be affected by the development of a capillary fringe
679 and (2) fluctuations in the groundwater water table, in addition to the typical (3) matric potential
680 above the tile pipe and (4) the soil saturated hydraulic conductivity considered by the steady-
681 state flow Hooghoudt's equation.

682

683 The groundwater table and matric potential changed dramatically between seasons, affecting
684 patterns of soil moisture and tile flow. Observations and model results showed that low
685 precipitation and higher evapotranspiration rates caused minimal tile flows during the crop-
686 growing season. Conversely, tile flow was often observed during the cold season, even during
687 small rainfall-runoff and snowmelt events due to a seasonal increase in the groundwater table
688 and soil saturated storage.

689

690 Model sensitivity tests showed that the capillary fringe strongly affected the amount of drainable
691 soil water flowing into the tile. Tile flow increased with drainable water, but the relationship is
692 highly non-linear likely because, as the tile carrying capacity is exceeded more frequently, there
693 is more opportunity time for groundwater seepage and evapotranspiration. Finally, observations
694 and model results reveal a bimodal soil saturated storage response in the presence of tiles, which
695 is controlled by the relative positioning of the capillary fringe in relation to the soil surface and
696 the depth of tile drains below the soil surface. Capturing these dynamics is a critical advance
697 enabling the accurate prediction of the swift hydrological changes caused by the presence of tiles
698 in models.

699 The TDM was developed as a first approximation from a single field site. Given this limitation, it
700 is not widely applicable across multiple field sites yet. However, the development of this module
701 has provided valuable insight into the potential for hourly time-step simulations, as well as the
702 importance of regional groundwater table fluctuations and simplifying the capillary fringe
703 parameters within models in some landscape types. Future work will include building on the
704 model and adapting it for different soil textures such as those in clay soils, where preferential
705 flow can have a strong impact on soil saturated storage and tile flow. Also, explicit

706 representation of unsaturated flow will be needed to enable the use of the model regions where
707 groundwater is disconnected from surface water, as commonly happens in arid and semi-arid
708 regions. Subsequent steps include the development of water quality modules.

709

710 **Code/Data availability**

711 The tile flow and soil water table data are not publicly available and will be provided upon
712 request to the data owner, Merrin Macrae. TDM code is not completely implemented in the main
713 version of the Cold Regions Hydrological Model platform and is provided only upon request to
714 the corresponding author.

715

716 **Author contribution**

717 MK and DC developed the model code and performed the simulations. MM prepared the data
718 and supported the field work. MK, DC and MM prepared the manuscript with contributions from
719 JP and RP.

720

721 **Competing interests**

722 The contact author has declared that none of the authors has any competing interests.

723

724 **Acknowledgements**

725 Funding for this project was provided by the Canada First Excellence Research Fund's Global
726 Water Futures programme through its Agricultural Water Futures project. Funding for the
727 collection of the field data was provided by the Ontario Ministry of Agriculture, Food and Rural

728 Affairs. The support of the Biogeochemistry Lab at the University of Waterloo for the collection
729 of field data and of Tom Brown and Xing Fang of the Centre for Hydrology at the University of
730 Saskatchewan for CRHM development and updates is gratefully acknowledged. The Maitland
731 Valley Conservation Authority is thanked for providing some precipitation, rainfall, and
732 temperature data.

733

734 **References**

735 Akis R.: Simulation of Tile Drain Flows in an Alluvial Clayey Soil Using HYDRUS 1D,
736 American-Eurasian J. Agric. & Environ. Sci., 16 (4), 801-813,
737 <https://doi.org/10.5829/idosi.ajeaes.2016.16.4.12906>, 2016.

738

739 Arheimer, B., Nilsson, J., and Lindstrom, G.: Experimenting with Coupled Hydro-Ecological
740 Models to Explore Measure Plans and Water Quality Goals in a Semi-Enclosed Swedish Bay,
741 Water, 7(7), 3906-3924, <https://doi.org/10.3390/w7073906>, 2015.

742

743 Arnold, J. G., Srinivasan, R., Muttiah, R. S., and Williams, J. R.: Large area hydrologic
744 modeling and assessment part I: model development, J. Am. Water. Resour. Assoc., 34, 73-89,
745 <https://doi.org/10.1111/j.1752-1688.1998.tb05961.x>, 1998.

746

747 Badr, A. W.: Physical properties of some North Carolina Organic Soils and the effect of land
748 development on these properties, M.S. Thesis, Department of Biological and Agricultural
749 Engineering, North Carolina State University, Raleigh, NC. 67 p., 1978.

750

751 Bleam, W. (2nd Edition): Soil and Environmental Chemistry, Academic Press, eBook ISBN:
752 9780128041956, 2017.
753

754 Bouwer, H. and van Schilfgaarde, J.: Simplified method of predicting the fall of water table in
755 drained land, Trans. ASAE. 6(4), 288-291, 296, 1963.
756

757 Brockley, R. P.: The effect of nutrient and moisture on soil nutrient availability, nutrient uptake,
758 tissue nutrient concentration, and growth of Douglas-Fir seedlings, Master Thesis, The
759 University of British Columbia, 1976.
760

761 Broughton, R. and Jutras, P.: Farm Drainage. In the Canadian Encyclopedia,
762 <https://www.thecanadianencyclopedia.ca/en/article/farm-drainage/>, last access: 14 February
763 2019.
764

765 Coelho, B. B., Murray, R., Lapen, D., Topp, E., and Bruin, A.: Phosphorus and sediment loading
766 to surface waters from liquid swine manure application under different drainage and tillage
767 practices, Agric. Water Manag., 104, 51-61, <https://doi.org/10.1016/j.agwat.2011.10.020>, 2012.
768

769 Cordeiro, M. R. C. and Ranjan, R. S.: Corn yield response to drainage and subirrigation in the
770 Canadian Prairies, Trans. ASABE. 55(5), 1771-1780, <https://doi.org/10.13031/2013.42369>,
771 2012.
772

773 Cordeiro, M. R. C., Wilson, H. F., Vanrobaeys, J., Pomeroy, J. W., Fang, X., and The Red-
774 Assiniboine Project Biophysical Modeling Team: Simulating cold-region hydrology in an
775 intensively drained agricultural watershed in Manitoba, Canada, using the Cold Region
776 Hydrological Model, *Hydrol. Earth Syst. Sci.*, 21, 3483-3506, [https://doi.org/10.5194/hess-21-](https://doi.org/10.5194/hess-21-3483-2017)
777 [3483-2017](https://doi.org/10.5194/hess-21-3483-2017), 2017.

778
779 Correll, D.: The role of phosphorus in the eutrophication of receiving waters: a review, *J.*
780 *Environ. Qual.*, 27, 261-266, <https://doi.org/10.2134/jeq1998.00472425002700020004x>, 1998.

781
782 Costa D., Klenk K., Knoblen W., Ireson A., Spiteri, R., Clark, M.: A multi-chemistry modelling
783 framework to enable flexible and reproducible water quality simulations in existing hydro-
784 models: 1. The OpenWQ concept and the water quality modelling lab. ESS Open Archive.
785 <https://10.22541/essoar.168718167.75677635/v1>, 2023

786
787 Diogo Costa, Kyle Klenk, Wouter Johannes Maria Knoblen, et al. A multi-chemistry modelling
788 framework to enable flexible and reproducible water quality simulations in existing hydro-
789 models: 2. The OpenWQ-SUMMA and OpenWQ-CRHM model implementations and testing.
790 ESS Open Archive. <https://10.22541/essoar.168652285.59958331/v1>, 2023.

791
792 Costa, D., Sutter, D., Shepherd, A., Jarvie, H., Wilson, H., Elliott, J., Liu, J., and Macrae, M.:
793 Impact of climate change on catchment nutrient dynamics: insights from around the
794 world. *Environmental Reviews*. **31**(1): 4-25. <https://doi.org/10.1139/er-2021-0109>, 2022

795

796 Costa, D., Baulch, H., Elliott, J., Pomeroy, J., and Wheeler, H.: Modelling nutrient dynamics in
797 cold agricultural catchments: A review, *Environ. Model. Softw.*, 124, 104586,
798 <https://doi.org/10.1016/j.envsoft.2019.104586>, 2020a.

799
800 Costa, D., Shook, K., Spence, C., Elliott, J., Baulch, H., Wilson, H., and Pomeroy, J.: Predicting
801 variable contributing areas, hydrological connectivity, and solute transport pathways for a
802 Canadian Prairie basin, *Water Resour. Res.*, 56, 1-23, <https://doi.org/10.1029/2020WR02798>,
803 2020b.

804
805 Costa, D., Burlando, P., Liong, S.-Y.: Coupling spatially distributed river and groundwater
806 transport models to investigate contaminant dynamics at river corridor scales. *Environmental*
807 *Modelling & Software*, 86, 91–110. <https://doi.org/10.1016/j.envsoft.2016.09.009>, 2016

808
809 Costa, D., Pomeroy, J. W., Brown, T., Baulch, H., Elliott, J., and Macrae, M.: Advances in the
810 simulation of nutrient dynamics in cold climate agricultural basins: Developing new nitrogen and
811 phosphorus modules for the Cold Regions Hydrological Modelling Platform, *J. Hydrol.*, 603, 1-
812 17, <https://doi.org/10.1016/j.jhydrol.2021.126901>, 2021.

813
814 Clark, M. P., Nijssen, B., Lundquist, J. D., Kavetski, D., Rupp, D. E., Woods, R. A., Freer, J. E.,
815 Gutmann, E. D., Wood, A. W., Brekke, L. D., Arnold, J. R., Gochis, D. J., & Rasmussen, R. M.
816 (2015). A unified approach for process-based hydrologic modeling: 1. Modeling concept. *Water*
817 *Resources Research*, 51(4), 2498–2514. <https://doi.org/https://doi.org/10.1002/2015WR017198>

818

819 Clark, M. P., Nijssen, B., Lundquist, J. D., Kavetski, D., Rupp, D. E., Woods, R. A., Freer, J. E.,
820 Gutmann, E. D., Wood, A. W., Gochis, D. J., Rasmussen, R. M., Tarboton, D. G., Mahat, V.,
821 Flerchinger, G. N., & Marks, D. G. (2015). A unified approach for process-based hydrologic
822 modeling: 2. Model implementation and case studies. *Water Resources Research*, 51(4), 2515–
823 2542. [https://doi.org/https://doi.org/10.1002/2015WR017200](https://doi.org/10.1002/2015WR017200)
824
825 De Ridder, N. A., Takes, C. A. P., van Someren, C. L., Bos, M. G., Messemaeckers van de
826 Graaff, R. H., Bokkers, A. H. J., Stransky, J., Wiersma-Roche, M. F. L., and Beekman, T.:
827 Drainage Principles and Applications. International Institute for Lan Reclamation and
828 Improvement, P.O. Box 45 Wageningen The Netherlands, 1974.
829
830 Du, B., Arnold, J. G., Saleh, A., and Jaynes, D. B.: Development and application of SWAT to
831 landscapes with tiles and potholes, *Trans. ASAE*, 48, 1121-1133,
832 <https://doi.org/10.13031/2013.18522>, 2005.
833
834 Du, B., Saleh, A., Jaynes, D. B., and Arnold, J. G.: Evaluation of SWAT in simulating nitrate
835 nitrogen and atrazine fates in a watershed with tiles and potholes, *Trans. ASABE*, 49, 949-959,
836 <https://doi.org/10.13031/2013.21746>, 2006.
837
838 ECCC, Canadian Climate Normals 1981-2010 Station Data,
839 [https://climate.weather.gc.ca/climate_normals/results_1981_2010_e.html?searchType=stnProx&
840 txtRadius=25&selCity=&selPark=&optProxType=custom&txtCentralLatDeg=43&txtCentralLat
841 Min=41&txtCentralLatSec=55&txtCentralLongDeg=81&txtCentralLongMin=28&txtCentralLon](https://climate.weather.gc.ca/climate_normals/results_1981_2010_e.html?searchType=stnProx&txtRadius=25&selCity=&selPark=&optProxType=custom&txtCentralLatDeg=43&txtCentralLatMin=41&txtCentralLatSec=55&txtCentralLongDeg=81&txtCentralLongMin=28&txtCentralLon)

842 [gSec=47&txtLatDecDeg=&txtLongDecDeg=&stnID=4545&dispBack=0](https://climate.weather.gc.ca/climate_data/daily_data_e.html?hlyRange=%7C&dlyRange=1966-06-01%7C2021-06-14&mlyRange=1966-01-01%7C2006-12-01&StationID=4603&Prov=ON&urlExtension=_e.html&searchType=stnName&optLimit=yearRange&StartYear=1840&EndYear=2022&selRowPerPage=25&Line=0&searchMethod=contains&Month=6&Day=4&txtStationName=Wroxeter&timeframe=2&Year=2021), last access: 5
843 February 2020.
844
845 Eckersten, H., Jansson, P. -E., and Johnsson, H. (2nd edition): SOILN model-user's manual,
846 Division of Agricultural Hydrotechnics Communications 94:4, Department of soil Sciences,
847 Swedish University of Agricultural Sciences, 58pp, Uppsala, 1994.
848
849 Environment Canada, Canadian Climate Normals 1981-2010 Station Data,
850 [https://climate.weather.gc.ca/climate_data/daily_data_e.html?hlyRange=%7C&dlyRange=1966-](https://climate.weather.gc.ca/climate_data/daily_data_e.html?hlyRange=%7C&dlyRange=1966-06-01%7C2021-06-14&mlyRange=1966-01-01%7C2006-12-01&StationID=4603&Prov=ON&urlExtension=_e.html&searchType=stnName&optLimit=yearRange&StartYear=1840&EndYear=2022&selRowPerPage=25&Line=0&searchMethod=contains&Month=6&Day=4&txtStationName=Wroxeter&timeframe=2&Year=2021)
851 [06-01%7C2021-06-14&mlyRange=1966-01-01%7C2006-12-](https://climate.weather.gc.ca/climate_data/daily_data_e.html?hlyRange=%7C&dlyRange=1966-06-01%7C2021-06-14&mlyRange=1966-01-01%7C2006-12-01&StationID=4603&Prov=ON&urlExtension=_e.html&searchType=stnName&optLimit=yearRange&StartYear=1840&EndYear=2022&selRowPerPage=25&Line=0&searchMethod=contains&Month=6&Day=4&txtStationName=Wroxeter&timeframe=2&Year=2021)
852 [01&StationID=4603&Prov=ON&urlExtension=_e.html&searchType=stnName&optLimit=year](https://climate.weather.gc.ca/climate_data/daily_data_e.html?hlyRange=%7C&dlyRange=1966-06-01%7C2021-06-14&mlyRange=1966-01-01%7C2006-12-01&StationID=4603&Prov=ON&urlExtension=_e.html&searchType=stnName&optLimit=yearRange&StartYear=1840&EndYear=2022&selRowPerPage=25&Line=0&searchMethod=contains&Month=6&Day=4&txtStationName=Wroxeter&timeframe=2&Year=2021)
853 [Range&StartYear=1840&EndYear=2022&selRowPerPage=25&Line=0&searchMethod=contain](https://climate.weather.gc.ca/climate_data/daily_data_e.html?hlyRange=%7C&dlyRange=1966-06-01%7C2021-06-14&mlyRange=1966-01-01%7C2006-12-01&StationID=4603&Prov=ON&urlExtension=_e.html&searchType=stnName&optLimit=yearRange&StartYear=1840&EndYear=2022&selRowPerPage=25&Line=0&searchMethod=contains&Month=6&Day=4&txtStationName=Wroxeter&timeframe=2&Year=2021)
854 [s&Month=6&Day=4&txtStationName=Wroxeter&timeframe=2&Year=2021](https://climate.weather.gc.ca/climate_data/daily_data_e.html?hlyRange=%7C&dlyRange=1966-06-01%7C2021-06-14&mlyRange=1966-01-01%7C2006-12-01&StationID=4603&Prov=ON&urlExtension=_e.html&searchType=stnName&optLimit=yearRange&StartYear=1840&EndYear=2022&selRowPerPage=25&Line=0&searchMethod=contains&Month=6&Day=4&txtStationName=Wroxeter&timeframe=2&Year=2021), last access: 10
855 May 2020.
856
857 Fang, X., Pomeroy, J. W., Westbrook, C. J., Guo, X., Minke, A. G., and Brown, T.: Prediction of
858 snowmelt derived streamflow in a wetland dominated prairie basin, Hydrol. Earth Syst. Sci., 14,
859 991-1006, <https://doi.org/10.5194/hess-14-991-2010>, 2010.
860
861 Fang, X., Pomeroy, J. W., Ellis, C. R., MacDonald, M. K., DeBeer, C. M., and Brown, T.: Multi-
862 variable evaluation of hydrological model predictions for a headwater basin in the Canadian
863 Rocky Mountains, Hydrol. Earth Syst. Sci., 17, 1635-1659, [https://doi.org/10.5194/hess-17-](https://doi.org/10.5194/hess-17-1635-2013)
864 [1635-2013](https://doi.org/10.5194/hess-17-1635-2013), 2013.

865

866 Filippelli, G. M.: The global phosphorus cycle, *Rev. Mineral. and Geochem.*, 48, 391-425,
867 <https://doi.org/10.2138/rmg.2002.48.10>, 2002.

868

869 Frey, S. K., Hwang, H. T., Park, Y. J., Hussain, S. I., Gottschall, N., Edwards, M., and Lapen, D.
870 R.: Dual permeability modeling of tile drain management influences on hydrologic and nutrient
871 transport characteristics in macroporous soil, *J. Hydrol.*, 535, 392-406,
872 <http://dx.doi.org/10.1016/j.jhydrol.2016.01.073>, 2016.

873

874 Gentry, L. E., David, M. B., Royer, T. V., Mitchell, C. A., and Starks, K.: Phosphorus transport
875 pathways to streams in tile-drained agricultural watersheds, *J. Environ. Quality.*, 36, 408-415,
876 <https://doi.org/10.2134/jeq2006.0098>, 2007.

877

878 Garcia-Gutierrez, C., Pachepsky, Y., and Martin, M. A.: Technical note: Saturated hydraulic
879 conductivity and textural heterogeneity of soils, *Hydrol. Earth Syst. Sci.*, 22, 3923-3932,
880 <https://doi.org/10.5194/hess-22-3923-2018>, 2018.

881

882 Green, C. H., Tomer, M. D., Di Luzio, M., and Arnold, J. G.: Hydrologic evaluation of the Soil
883 and Water Assessment Tool for large tile-drained watershed in Iowa, *Trans. ASABE.*, 49, 413-
884 422, <https://doi.org/10.13031/2013.20415>, 2006.

885

886 Hansen, A. L., Jakobsen, R., Refsgaard, J. C., Hojberg, A. L., Iversen, B. V., and Kjaergaard, C.:
887 Groundwater dynamics and effect of tile drainage on water flow across the redox interface in a

888 Danish Weichsel till area, *Advances in Water Resources*, 123, 23-39,
889 <https://doi.org/10.1016/j.advwatres.2018.10.022>, 2019.

890

891 Hirt, U., Wetzig, A., Amatya, M. D., and Matranga, M.: Impact of seasonality on artificial
892 drainage discharge under temperate climate conditions, *Int. Rev. Hydrobiol.*, 96, 561-577,
893 <https://doi.org/10.1002/iroh.201111274>, 2011.

894

895 Hooghoudt, S. B.: Bijdrage tot de kennis van enige natuurkundige grootheden van de grand.
896 *Verslagen van Landbouwkundige Onderzoekingen*, 46(7), 515-707, the Hague, The Netherlands
897 (in Dutch), 1940.

898

899 ICID: World Drained Area-2018. International Commission on Irrigation and Drainage.
900 <http://www.icid.org/world-drained-area.pdf> , last access: 14 February 2019.

901

902 Jamieson, A., Madramootoo, C. A., and Enright, P.: Phosphorus losses in surface and subsurface
903 runoff from a snowmelt event on an agricultural field in Quebec, *Can. Biosyst. Eng.*, 45, 11-17,
904 2003.

905

906 Jarvie, H. P., Johnson, L. T., Sharpley, A. N., Smith, D. R., Baker, D. B., Bruulsema, T. W., and
907 Confesor, R.: Increased Soluble Phosphorus Loads to Lake Erie: Unintended Consequences of
908 Conservation Practices?, *J. Environ. Qual.*, 46, 123-132,
909 <https://doi.org/10.2134/jeq2016.07.0248>, 2017.

910

911 Javani-Jouni, H., Liaghat, A., Hassanoghli, A., and Henk, R.: Managing controlled drainage in
912 irrigated farmers' fields: A case study in the Moghan Plain, Iran, *Agric. Water Manag.*, 208, 393-
913 405, <https://doi.org/10.1016/j.agwat.2018.06.037>, 2018.

914

915 Johnsen, K. E., Liu, H. H., Dane, J. H., Ahuja, L. R., and Workman, S. R.: Simulating
916 Fluctuating Water Tables and Tile Drainage with a Modified Root Zone Water Quality Model
917 and a New Model WAFLOWM, *Transactions of the ASAE*, 38 (1), 75-83,
918 <https://doi.org/10.10031/2013.27814>, 1995.

919

920 Kiesel, J., Fohrer, N., Schmalz, B., and White, M. J.: Incorporating landscape depressions and
921 tile drainages of a northern German lowland catchment into a semi-distributed model, *Hydrol.*
922 *Process.*, 24, 1472-1486, <https://doi.org/10.1002/hyp.7607>, 2010.

923

924 King, K. W., Williams, M. R., Macrae, M. L., Fausey, N. R., Frankenberger, J., Smith, D. R.,
925 Kleinman, P. A. J., and Brown, L. C.: Phosphorus transport in agricultural subsurface drainage:
926 A review, *J. Environ. Qual.*, 44(2), 467-485, <https://doi.org/10.2134/jeq2014.04.0163>, 2015.

927

928 King, K. W., Williams, M. R., and Fausey, N. R.: Effect of crop type and season on nutrient
929 leaching to tile drainage under a corn-soybean rotation, *J. Soil and Water Conserv.*, 71, 56-68,
930 <https://doi.org/10.2489/jswc.71.1.56>, 2016.

931

932 Kirkham, D.: Theory of land drainage, in, *Drainage of Agricultural Lands*. Agronomy
933 Monograph, No. 7, American Society of Agronomy, Madison, Wisconsin, 1957.

934

935 Kladivko, E. J., Grochulska, J., Turco, R. F., Van Scoyoc, G. E., and Eigel, J. D.: Pesticide and
936 nitrate transport into subsurface tile drains of different spacings, *J. Environ. Qual.*, 28, 997-1004,
937 <https://doi.org/10.2134/jeq1999.00472425002800030033x>, 1999.

938

939 Klaiber, L. B., Kramer, S. R., and Young, E. O.: Impacts of Tile Drainage on Phosphorus Losses
940 from Edge-of-field Plots in the Lake Champlain Basin of New York, *Water*, 12, 328,
941 <https://doi.org/10.3390/w12020328>, 2020.

942

943 Kock, S., Bauwe, A., and Lennartz, B.: Application of SWAT Model for a Tile-Drained Lowland
944 Catchment in North-Eastern Germany on Subbasin Scale, *Water Resour. Manage.*, 27, 791-805,
945 <https://doi.org/10.1007/s11269-012-0215-x>, 2013.

946

947 Kokulan, V.: Environmental and Economic Consequences of Tile Drainage Systems in Canada,
948 The Canadian Agri-Food Policy Institute (CAPI), 2019.

949

950 Kokulan, V., Macrae, M. L., Ali, G. A., and Lobb, D. A.: Hydroclimatic controls on runoff
951 activation in a artificially drained, near-level vertisolic clay landscape in a Prairie climate, *Hyrol.*
952 *Process.*, 33, 602-615, <https://doi.org/10.1002/hyp.13347>, 2019a.

953

954 Lam, W. V., Macrae, M. L., English, M. C., O'Halloran, I. P., Plach, J. M., and Wang, Y.:
955 Seasonal and event-based drives of runoff and phosphorus export through agricultural tile drains

956 under sandy loam soil in a cool temperate region, *Hydrol. Process.*, 30, 2644-2656,
957 <https://doi.org/10.1002/hyp.10871>, 2016a.

958

959 Lam, W. V., Macrae, M. L., English, M. C., O'Halloran, I., and Wang, Y.: Effects of tillage
960 practices on phosphorus transport in tile drain effluent in sandy loam agricultural soils in
961 Ontario, Canada, *J. Great Lakes Res.*, 42(6), 1260-1270,
962 <https://dx.doi.org/10.1016/j.jglr.2015.12.015>, 2016b.

963

964 Larsbo, M., and Jarvis, N.: MACRO 5.0. A model of water flow and solute transport in
965 microporous soil, Technical description. Swedish University of Agricultural Sciences, Division
966 of Environmental Physics, Emergo 2003:6 Report, ISSN 1651-7210, ISBN 91-576-6592-3,
967 2003.

968

969 Lindstrom, G., Pers, C., Rosberg, J., Stromqvist, J., and Arheimer, B.: Development and testing
970 of the HYPE (Hydrological Predictions for the Environment) water quality model for different
971 scales, *Hydrol. Res.*, 41(3-4), 295-319, <https://doi.org/10.2166/nh.2010.007>, 2010.

972

973 Logsdon, S. D., Schilling, K. E., Hernandez-Ramirez, G., Prueger, J. H., Hatfield, J. L., and
974 Sauer, T. J.: Field estimation of specific yield in a central Iowa crop field, *Hydrol. Process.*, 24,
975 1369-1377, <https://doi.org/10.1002/hyp.7600>, 2010.

976

977 Macrae, M. L., English, M. C., Schiff, S. L., and Stone, M. L.: Intra-annual variability in the
978 contribution of tile drains to basin discharge and phosphorus export in a first order agricultural

979 catchment, *Agric. Water Manag.*, 92, 171-182, <https://doi.org/10.1016/j.agwat.2007.05.015>,
980 2007.
981
982 Macrae, M. L., Ali, G. A., King, K. W., Plach, J. M., Puer, W. T., Williams, M., Morison, M.
983 Q., and Tang, W.: Evaluating Hydrologic Response in Tile-Drained Landscapes: Implications for
984 Phosphorus Transport, *J. Environ. Qual.*, 48(5), 1347-1355,
985 <https://doi.org/10.2134/jeq2019.02.0060>, 2019.
986
987 Malzone, J. M., Lowry, C. S., and Ward, A. S.: Response of the hyporheic zone to transient
988 groundwater fluctuations on the annual and storm event time scales, *Water Resour. Res.*, 52,
989 5301-5321, <https://doi.org/10.1002/2015WR018056>, 2016.
990
991 Mizukami, N., Clark, M. P., Sampson, K., Nijssen, B., Mao, Y., McMillan, H., Viger, R. J.,
992 Markstrom, S. L., Hay, L. E., Woods, R., Arnold, J. R., & Brekke, L. D. (2016). mizuRoute
993 version 1: A river network routing tool for a continental domain water resources applications.
994 *Geoscientific Model Development*, 9, 2223–2238. <https://doi.org/10.5194/gmd-9-2223-2016>
995 Moriasi, D. N., Arnold, J. G., Van Liew, M. W., Bingner, R. L., Harmel, R. D., and Veith, T. L.:
996 Model Evaluation Guidelines for Systematic Quantification of Accuracy in Watershed
997 Simulations, *Trans. ASABE*, 50(3), 885-900, <https://doi.org/10.13031/2013.23153>, 2007.
998
999 Moriasi, D. N., Gowda, P. H., Arnold, J. G., Mulla, D. J., Ale, S., Steiner, J. L., and Tomer, M.
1000 D.: Evaluation of the Hooghoudt and Kirkham Tile Drain Equations in the Soil and Water

1001 Assessment Tool to Simulate Tile Flow and Nitrate-Nitrogen, *J. Environ. Qual.*, 42, 1699-1710,
1002 <https://doi.org/10.2134/jeq2013.01.0018>, 2013.

1003

1004 Plach, J. M., Macrae, M. L., Ali, G. A., Brunke, R. R., English, M. C., Ferguson, G., Lam, W.
1005 V., Lozier, T. M., McKague, K., O'Halloran, I. P., Opolko, G., and Van Esbroeck, C. J.: Supply
1006 and Transport Limitations on Phosphorus Losses from Agricultural Fields in the Lower Great
1007 Lakes Region, Canada, *J. Environ. Qual.*, 47, 96-105, <https://doi.org/10.2134/jeq2017.06.0234>,
1008 2018a.

1009

1010 Plach, J. M., Macrae, M. L., Williams, M. R., Lee, B. D., and King, K. W.: Dominant glacial
1011 landforms of the lower Great Lakes region exhibit different soil phosphorus chemistry and
1012 potential risk for phosphorus loss, *J. Great Lakes Res.*, 44, 1057-1067,
1013 <https://doi.org/10.1016/j.jglr.2018.07.005>, 2018b.

1014

1015 Plach, J., Puer, W., Macrae, M., Kompanizare, M., McKague, K., Carlow, R., and Brunke, R.:
1016 Agricultural Edge of Field Phosphorus Losses in Ontario, Canada: Importance of the
1017 Nongrowing Season in Cold Regions, *J. Environ. Qual.*, 48, 813-821,
1018 <https://doi.org/10.2134/jeq2018.11.0418>, 2019.

1019

1020 Puer, W. T., Macrae, M., Buckley, A., and Reid, K.: Contribution of preferential flow to tile
1021 drainage varies spatially and temporally, *Vadose Zone J.*, 19: e20043,
1022 <https://doi.org/10.1002/vzj2.20043>, 2020.

1023

1024 Pomeroy, J. W., Gray, D. M., Shook, K. R., Toth, B., Essery, R. L. H., Pietroniro, A., and
1025 Hedstrom, N. R.: An evaluation of snow accumulation and ablation processes for land surface
1026 modelling, Hydrol. Process., 12, 2339-2367, [https://doi.org/10.1002/\(SICI\)1099-](https://doi.org/10.1002/(SICI)1099-1085(199812)12:15)
1027 [1085\(199812\)12:15](https://doi.org/10.1002/(SICI)1099-1085(199812)12:15), 1998.

1028

1029 Pomeroy, J. W., Gray, D. M., Brown, T., Hedstrom, N. R., Quinton, W. L., Granger, R. J., and
1030 Carey, S. K.: The cold regions hydrological model: a platform for basing process representation
1031 and model structure on physical evidence, Hydrol. Process., 21, 2650-2667,
1032 <https://doi.org/10.1002/hyp.6787>, 2007.

1033

1034 Pomeroy, J. W., Fang, X., Shook, K., and Whitfield, P. H.: Predicting in Ungauged Basins Using
1035 Physical Principles Obtained Using the Deductive, Inductive, and Abductive Reasoning
1036 Approach, [https://research-](https://research-groups.usask.ca/hydrology/documents/pubs/papers/pomeroy_et_al_2003_3.pdf)
1037 [groups.usask.ca/hydrology/documents/pubs/papers/pomeroy et al 2003 3.pdf](https://research-groups.usask.ca/hydrology/documents/pubs/papers/pomeroy_et_al_2003_3.pdf) , 2013.

1038

1039 Pomeroy, J. W., Fang, X., and Marks, D. G.: The cold rain-on-snow event of June 2013 in the
1040 Canadian Rockies - characteristics and diagnosis, Hydrol. Process., 30, 2899-2914,
1041 <https://doi.org/10.1002/hyp.10905>, 2016.

1042

1043 Pomeroy, J. W., Brown, T., Fang, X., Shook, K. R., Pradhananga, D., Armstrong, R., Harder, P.,
1044 Marsh, C., Costa, D., Krogh, S. A., Aubry-Wake, C., Annand, H., Lawford, P., He, Z.,
1045 Kompanizare, M., and Lopez Moreno, J. I.: The cold regions hydrological modelling platform

1046 for hydrological diagnosis and prediction based on process understanding, *J. of Hydrol.*, 615 (A),
1047 128711, <https://doi.org/10.1016/j.jhydrol.2022.128711>, 2022.

1048

1049 Qi, P., Zhang, G., Xu, Y. J., Wang, L., Ding, C., and Cheng, C.: Assessing the Influence of
1050 Precipitation on Shallow Groundwater Table Response Using Combination of Singular Value
1051 Decomposition and Cross-Wavelet Approaches, *Water*, 10, 598,
1052 <https://doi.org/10.3390/w10050598>, 2018.

1053

1054 Quinton, J. G., Govers, G., van Oost, K., and Bardgett, R.: The impact of agricultural soil erosion
1055 on biochemical cycling, *Nat. Geosci.*, 3, 311-314, <https://doi.org/10.1038/ngeo838>, 2010.

1056

1057 Raats, P. A. C. and Gardner, W. R.: Movement of water in saturated zone near a water table. Ch.
1058 13 in *Drainage for agriculture*, J. van Schilfgraade, Ed., *Agronomy Monograph*. No. 17,
1059 American Society of Agronomy, Madison, WI, pp. 331-357, 1974.

1060

1061 Radcliffe, D. E., Reid, D. K., Blomback, K., Bolster, C. H., Collick, A. S., Easton, Z. M.,
1062 Francesconi, W., Fuka, D. R., Johnsson, H., King, K., Larsbo, M., Youssef, M. A., Mulkey, A.
1063 S., Nelson, N. O., Persson, K., Ramirez-Avila, J. J., Schmieder, F., and Smith, D. R.:
1064 Applicability of Models to Predict Phosphorus Losses in Drained Fields: A Review, *J. Environ.*
1065 *Qual.*, 44, 614-628, <https://doi.org/10.2134/jeq2014.05.0220>, 2015.

1066

1067 Rahman, M. M., Lin, Z., Jia, X., Steele, D. D., and DeSutter, T. M.: Impact of subsurface
1068 drainage on streamflows in Red River of the North basin, *J. Hydrol.*, 511, 474-483,
1069 <https://doi.org/10.1016/j.jhydrol.2014.01.070>, 2014.
1070
1071 Refsgaard, J. C. and Storm, B.: MIKE SHE. In: Singh VP (ed) Computer models of watershed
1072 hydrology, Highlands Ranch, Water Research Pub, Colorado, 1995.
1073
1074 Richards L. A.: Capillary conduction of liquids through porous medium, *Physics*, 1 (5): 318-333,
1075 Bibcode:1931Physi...1..318R. <https://doi.org/10.1063/1.1745010>, 1931.
1076
1077 Rozemeijer, J. C., Visser, A., Borren, W., Winegram, M., van der Velde, Y., Klein, J., and
1078 Broers, H. P.: High-frequency monitoring of water fluxes and nutrient loads to assess the effects
1079 of controlled drainage on water storage and nutrient transport, *Hydrol. Earth Syst. Sci.*, 20, 347-
1080 358, <https://doi.org/10.5194/hess-20-347-2016>, 2016.
1081
1082 Rust, W., Holman, I., Bloomfield, J. Cuthbert, M., and Corstanje, R.: Understanding the potential
1083 of climate teleconnections to project future groundwater drought, *Hydrol. Earth Syst. Sci.*, 23,
1084 3233-3245, <https://doi.org/10.5194/hess-23-3233-2019>, 2019.
1085
1086 Ruttenberg, K.: The global phosphorus cycle. In *Biochemistry*, Vol. 8, treatise on geochemistry,
1087 Schlesinger W (ed) (eds. H. Holland and K. Turekian). Elsevier-Pergamon: Oxford; 585-643,
1088 2005.
1089

1090 Searcy, J. and Hardison, C. H.: Double –Mass Curves. Manual of Hydrology: Part 1, General
1091 Surface-Water Techniques, Geological Survey Water-Supply Paper 1541-B, 1960.
1092
1093 Schindler, D. W.: Recent advances in the understanding and management of eutrophication,
1094 Limnol. Oceanogr., 51, 356-363, https://doi.org/10.4319/lo.2006.51.1_part_2.0356, 2006.
1095
1096 Sharpley, A. N., Hedley, M. J., Sibbesen, E., Hillbricht-Ilkowska, A., House, W. A., and
1097 Ryszkowski, L.: Phosphorus transfer from terrestrial to aquatic ecosystems, In Phosphorus in the
1098 global environment, Tiessen H (ed), Scientific Committee on Problems of the Environment
1099 (SCOPE). John Wiley & SonsLtd.: Chichester; 171-199, 1995.
1100
1101 Simunek J., van Genuchten M. Th., and Sejna M.: The HYDRUS Software Package for
1102 Simulating Two- and Three-Dimensional Movement of Water, Heat and Multiple Solutes in
1103 Variably-Saturated Media, Technical Manual, Version 2.0, PC Progress, Prague, Czech
1104 Republic, pp. 258, 2011.
1105
1106 Skaggs, R. W.: A water management model for shallow water table soils, University of North
1107 Carolina, Water Resource Research Institute, Technical Report 134, 1978.
1108
1109 Skaggs, R. W.: Combination surface-subsurface drainage systems for humid regions. J. Irrig.
1110 Drain. Div., ASCE. 106(IR4), 265-283, 1980a.
1111

1112 Skaggs, R. W.: Drainmod Reference Report, Methods for Design and Evaluation of Drainage-
1113 Water Management Systems for Soils with High Water Tables, U.S. Department of Agriculture,
1114 Soil Conservation Service, North Carolina State University, Raleigh, North Carolina, 1980b.
1115
1116 Skaggs, R. W., Wells, L. G., and Ghate, S. R.: Predicted and measured drainable porosities for
1117 field soils, Trans. ASAE, 21(3), 522-528, https://uknowledge.uky.edu/bae_facpub/199, 1978.
1118
1119 Skaggs, R. W., Youssef, M. A., and Chescheir, G. M.: DRAINMOD: Model Use, Calibration,
1120 and Validation, Trans. ASABE, 55(4), 1509-1522, <https://doi.org/10.13031/2013.42259>, 2012.
1121
1122 Smedema, L. K., Vlotman, W. F., and Rycroft, D.: Modern land Drainage. Planning, design and
1123 management of agricultural drainage systems, London: Taylor & Francis.
1124 <https://doi.org/10.1201/9781003>, 2004.
1125
1126 Smith, D. R., King, K. W., Johnson, L., Francesconi, W., Richards, P., Baker, D., and Sharpley,
1127 A. N.: Surface runoff and tile drainage transport of phosphorus in the Midwestern United States,
1128 J. Environ. Qual., 44, 495-502, <https://doi.org/10.2134/jeq2014.04.0176>, 2015.
1129
1130 Tomer, M. D., Meek, D. W., Jaynes, D. B., and Hatfield, J. L.: Evaluation of nitrate nitrogen
1131 fluxes from a tile-drained watershed in Central Iowa, J. Environ. Qual., 32, 642-653,
1132 <https://doi.org/10.2134/jeq2003.6420>, 2003.
1133

1134 Twarakavi, N. K. C., Sakai, M., and Simunek, J.: An objective analysis of the dynamic nature of
1135 field capacity, *Water Resour. Res.*, 45, W10410, <https://doi.org/10.1029/2009WR007944>, 2009.
1136

1137 Van Esbroeck, C. J., Macrae, M. L., Brunke, R. I., and McKague, K.: Annual and seasonal
1138 phosphorus export in surface runoff and tile drainage from agricultural fields with cold temperate
1139 climates, *J. Great Lakes Res.*, 42(6), 1271-1280, <https://doi.org/10.1016/j.jglr.2015.12.014>, 2016.
1140

1141 Van Esbroeck, C. J., Macrae, M. L., Brunke, R. R., and McKague, K.: Surface and subsurface
1142 phosphorus export from agricultural fields during peak flow events over the nongrowing season
1143 in regions with cool, temperate climates, *Journal of Soil and Water Conservation*, 72(1), 65-76,
1144 <https://doi:10.2489/jswc.72.1.65> , 2017.
1145

1146 Van Schilfgaarde, J.: Nonsteady flow to drains, In *Drainage for Agriculture*, J. van Schilfgaarde,
1147 ed. American Society of Agronomy, Madison, WI. PP 245-270, 1974.
1148

1149 Vaughan, P. J., Suarez, D. L., Simunek, J., Corwin, D. L., and Rhoades, J. D.: Role of
1150 Groundwater Flow in Tile Drain Discharge, *J. Environ. Qual.*, 28, 403-410,
1151 <https://doi.org/10.2134/jeq1999.00472425002800020006x>, 1999.
1152

1153 Vidon, P. and Cuadra, P. E.: Impact of precipitation characteristics on soil hydrology in tile
1154 drained landscapes, *Hydrol. Process.*, 24, 1821-1833, <https://doi.org/10.1002/hyp.7627>, 2010.
1155

1156 Vivekananthan, K.: Environmental and Economic Consequences of Tile Drainage Systems in
1157 Canada, The Canadian Agri-Food Policy Institute, www.capi-icpa.ca, 2019.
1158

1159 Vivekananthan, K., Macrae, M., Lobb, D. A., and Ali, G. A.: Contribution of overland and tile
1160 flow to runoff and nutrient losses from vertisols in Manitoba, Canada, *J. Environ. Qual.*, 48(4),
1161 959-965, <https://doi.org/10.2134/jeq2019.03.0103>, 2019.
1162

1163 Waichler, S. R. and Wigmosta, M. S.: Development of Hourly Meteorological Values from
1164 Daily Data and Significance to Hydrological Modeling at H. J. Andrews Experimental Forest,
1165 *Am. Meteorol. Soc.*, 4, 251-263, [https://doi.org/10.1175/1525-
1166 7541\(2003\)4<251:DOHMFV>2.0.CO;2](https://doi.org/10.1175/1525-7541(2003)4<251:DOHMFV>2.0.CO;2), 2003.
1167

1168 Williams, M. R., King, K. W., and Fausey, N. R.: Drainage water management effects on tile
1169 discharge and water quality, *Agric. Water Manag.*, 148, 43-51,
1170 <http://dx.doi.org/10.1016/j.agwat.2014.09.017>, 2015.
1171

1172 Williams, M. R., King, K. W., Ford, W., Buda, A. R., and Kennedy, C. D.: Effect of tillage on
1173 macropore flow and phosphorus transport to tile drains, *Water Resour. Res.*, 52, 2868-2882,
1174 <https://doi.org/10.1002/2015WR017650>, 2016.
1175

1176 Williams, M. R., Livingston, S. J., Heathman, G. C., and McAfee, S. J.: Thresholds for run-off
1177 generation in a drained closed depression, *Hydrol. Process.*, 1-14,
1178 <https://doi.org/10.1002/hyp.13477>, 2019.

1179

1180 Youngs, E. G.: Effect of the Capillary fringe on Steady-State Water Tables in drained Lands, J.

1181 Irrig. Drain. Eng., 138(9), 809-814, [https://doi.org/10.1061/\(ASCE\)IR.1943-4774.0000467](https://doi.org/10.1061/(ASCE)IR.1943-4774.0000467),

1182 2012.

1183

1184

1185 **Appendix A**

1186 Table A1. Instrument names and descriptions

Instrument name	Description
Hach Flo-tote and FL900 logger	Flow velocity and water level measurement
U20, Onset Ltd.	Barometrically-corrected pressure transducer
Temperature Smart Sensor S-THB-M002	Air temperature measurement
Wind Smart Sensor S-WSET-M002	Wind speed measurement
(Silicon Pyranometer)-S-LIB-M003	Solar radiation sensor
Tipping bucketrain gauge, 0.2 mm Rainfall Smart Sensor – SRGB-M002	Rainfall measurement
RH Smart Sensor(S-THB-M002)	Relative Humidity measurement

1187

1188

1189

1190 **Appendix B**

1191 Table B1. Parameter names and their symbols in CRHM platform

Parameter symbol	Parameter name

Tair	Air temperature
Wspeed	Wind speed
RH	Relative Humidity
Qsi	Incoming solar irradiance
R	Rainfall
WQ_soil	Water Quality soil module
WT	Water table elevation above the semipermeable layer
SSS	Soil saturated storage or the saturated part of the soil moisture
soil_moist	Soil moisture
Porosity_soil	Soil porosity
AL	Above layer
BL	Below layer
GWRD	Groundwater level fluctuations, groundwater recharge and discharge

1192

1193

1194

1195 **Appendix C**

1196

1197 We show how we assess seasonal factors ($f_{y,i}$) for different years in this study. Equation (4) can

1198 be written as:

1199

1200 $G_{y,i} = G \times f_{y,i}$ (C1)

1201

1202 For each year (y), $f_{y,i}$ for the first ($f_{y,1}$) and second ($f_{y,2}$) part of the sine function (G), where

1203 $G \geq 0$ and $G < 0$ respectively, were defined as:

1204

$$1205 \begin{cases} \text{if } G \geq 0 [i = 1] \text{ then } f_{y,1} = x \\ \text{if } G < 0 [i = 2] \text{ then } f_{y,2} = y \end{cases} \quad (\text{C-2})$$

1206

1207 G is the sine function representing the annual fluctuations in water table (WT/SSS). So, for n

1208 years there are $n \times 2$ $f_{y,i}$ values. The default values for $f_{y,i}$ are 1 and the default values can be

1209 changed for each year and for first and second parts in each year independently. Calculated $G_{y,i}$

1210 in each time step add or subtracted to or from the total soil moisture depend on the its sign. The

1211 values for the sine function parameters are in Fig. C1. The verified sine function time series

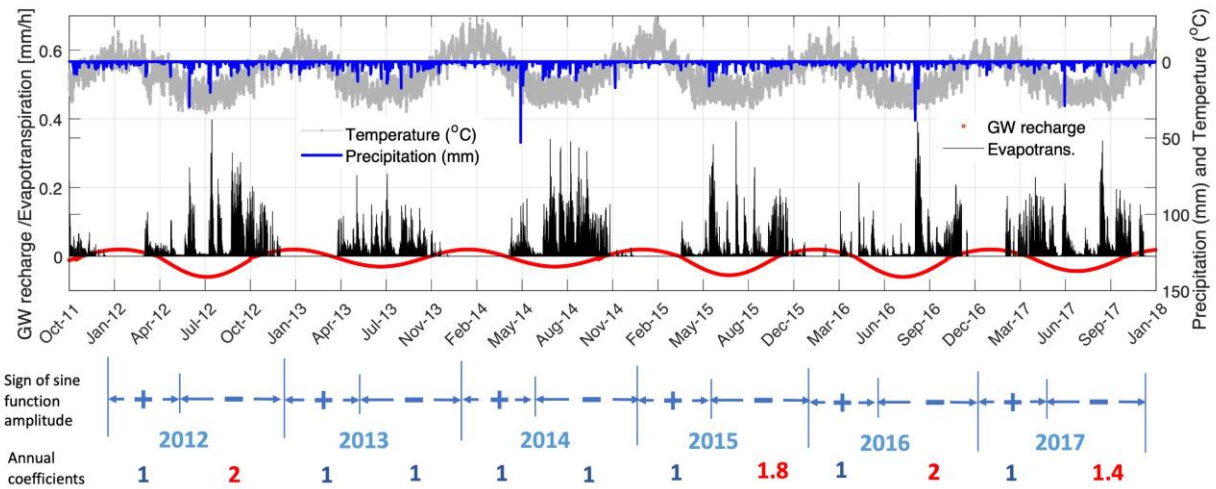
1212 along with time series of temperature, precipitation and calculated evapotranspiration are shown

1213 in Fig. C1. In this figure it is obvious that in years 2012 and 2015 to 2017 the warm season

1214 amplitudes are larger. The ET values are happened more in the warm seasons (growing seasons).

1215 Also, it can be seen that the seasonal oscillation in sine function is very similar to the

1216 temperature general oscillations.



1217

1218 Figure C1. Time series of the adjustable sine function along with the time series of calculated evapotranspiration, temperature
1219 and precipitation during the study period from Oct 2011 to Sept 2018.